

## THE ORIGIN OF COLD FRONTS IN THE CORES OF RELAXED GALAXY CLUSTERS

YAGO ASCASIBAR<sup>1</sup> AND MAXIM MARKEVITCH<sup>2</sup>

Harvard-Smithsonian Center for Astrophysics, 60 Garden St., Cambridge, MA 02138

Draft version October 12, 2018

### ABSTRACT

*Chandra* X-ray observations revealed the presence of cold fronts (sharp contact discontinuities between gas regions with different temperatures and densities) in the centers of many, if not most, relaxed clusters with cool cores. We use high-resolution simulations of idealized cluster mergers to show that they are due to sloshing of the cool gas in the central gravitational potential, which is easily set off by minor mergers and can persist for gigayears. The only necessary condition is a steep entropy profile, as observed in cooling flow clusters. Even if the infalling subcluster has no gas during core passage, the gravitational disturbance sets the main mass peak (gas and dark matter together) in motion relative to the surrounding gas. A rapid change in the direction of motion causes a change in ram pressure, which pushes the cool gas away from the dark matter peak and triggers sloshing. For nonzero impact parameters, the cool gas acquires angular momentum, resulting in a characteristic spiral pattern of cold fronts. There is little visible disturbance outside the cool core in such a merger. If the subcluster retains its gas during core passage, the cool central gas of the main cluster is more easily decoupled from the dark matter peak. Subsequently, some of that gas, and often the cool gas from the subcluster, falls back to the center and starts sloshing. However, in such a merger, global disturbances are readily visible in X-rays for a long time. We conclude that cold fronts at the centers of relaxed clusters, often spiral or concentric-arc in shape, are probably caused by encounters with small subhalos stripped of all their gas at the early infall stages.

*Subject headings:* galaxies: clusters: general – hydrodynamics – instabilities – methods: numerical – X-rays: galaxies: clusters

### 1. INTRODUCTION

High-resolution X-ray observations of galaxy clusters with the *Chandra* satellite revealed a number of interesting and unexpected features in the intracluster medium (ICM). Many clusters were found to exhibit sharp, arc-shaped, edge-like jumps in their gas density and temperature. Unlike in shock fronts, the gas on the dense side of these “cold fronts” is cooler, so the pressure is continuous across the front (e.g., Markevitch et al. 2000; Vikhlinin et al. 2001). Cold fronts are much more ubiquitous than shock fronts; only two convincing examples of the latter have been found so far (1E 0657–56 and A520), while cold fronts are observed in many if not most clusters. In merging systems, they were immediately interpreted as contact discontinuities between gases from different subclusters (Markevitch et al. 2000). In some cases, such as the cluster 1E 0657–56 or the galaxy NGC 1404, this is quite obvious from the X-ray and optical images which show that the cold front is a boundary of the cool gas belonging to the infalling subcluster (e.g., Markevitch et al. 2002; Machacek et al. 2005). However, cold fronts are also observed near the centers of cooling flow<sup>3</sup> clusters, many of which are relaxed and show little or no signs of recent merging (e.g., Mazzotta et al. 2001; Markevitch et al. 2001, 2003; Churazov et al. 2003; Dupke & White 2003; Sanders et al. 2005). These fronts are typically more subtle in terms of the density jump than those in mergers. Some of the examples are shown in Fig. 1; one of them is in A2029, which on scales  $r > 100$ –200 kpc is the most relaxed cluster known (e.g., Buote & Tsai 1996).

In these clusters, the moving gas clearly does not belong to any infalling subcluster. Markevitch et al. (2001) showed that the gas forming the cold front in A1795, another very relaxed cluster, is not in hydrostatic equilibrium and proposed that the front is caused by subsonic “sloshing” of the cluster’s own central gas in the gravitational potential well as a result of a disturbance of the central potential by past subcluster infall, or a gas disturbance from the central AGN activity. It is important to establish the nature of these features, because they may have significant effect on the energy balance in the cooling flows, as well as on estimates of the cluster total mass based on the assumption of hydrostatic equilibrium.

In this work, we wish to test whether gas sloshing in the cluster cores can create cold fronts and investigate the possible origin of such sloshing. We use high-resolution numerical simulations of idealized cluster mergers to explore the possibility that such features are a long-lived consequence of the infall of small subclusters. We will be particularly interested in determining whether it is possible for a merger to create cold fronts in the cool core, without significantly disturbing the ICM as a whole.

Several earlier works analyzed cluster mergers found in cosmological simulations and demonstrated that cold fronts can indeed form as a result of ram-pressure stripping and subsequent adiabatic expansion of the cold gas belonging to merging subclusters (Bialek et al. 2002; Nagai & Kravtsov 2003; Mathis et al. 2005). Detailed effects of ram-pressure stripping on a substructure moving through the ICM have also been studied using idealized 3D or 2D merger simulations (e.g. Heinz et al. 2003; Acreman et al. 2003; Asai et al. 2004; Takizawa 2005, among others). Closer to the questions that we wish to address here, Churazov et al. (2003) and Fujita et al. (2004) used 2D simulations to model a weak shock or acoustic wave propagating toward the cluster center. They found that it can displace the cool gas from the gravitational

<sup>1</sup> Presently at the Astrophysikalisches Institut Potsdam, An der Sternwarte 16, D-14482 Potsdam, Germany; yago@aip.de

<sup>2</sup> Also Space Research Institute, Russian Acad. Sci., Profsoyuznaya 84/32, Moscow 117997, Russia

<sup>3</sup> For the purpose of this work, we will use the term “cooling flow” simply to denote the observed centrally peaked gas density and temperature profiles, fully aware of the problems of the physical cooling flow model.

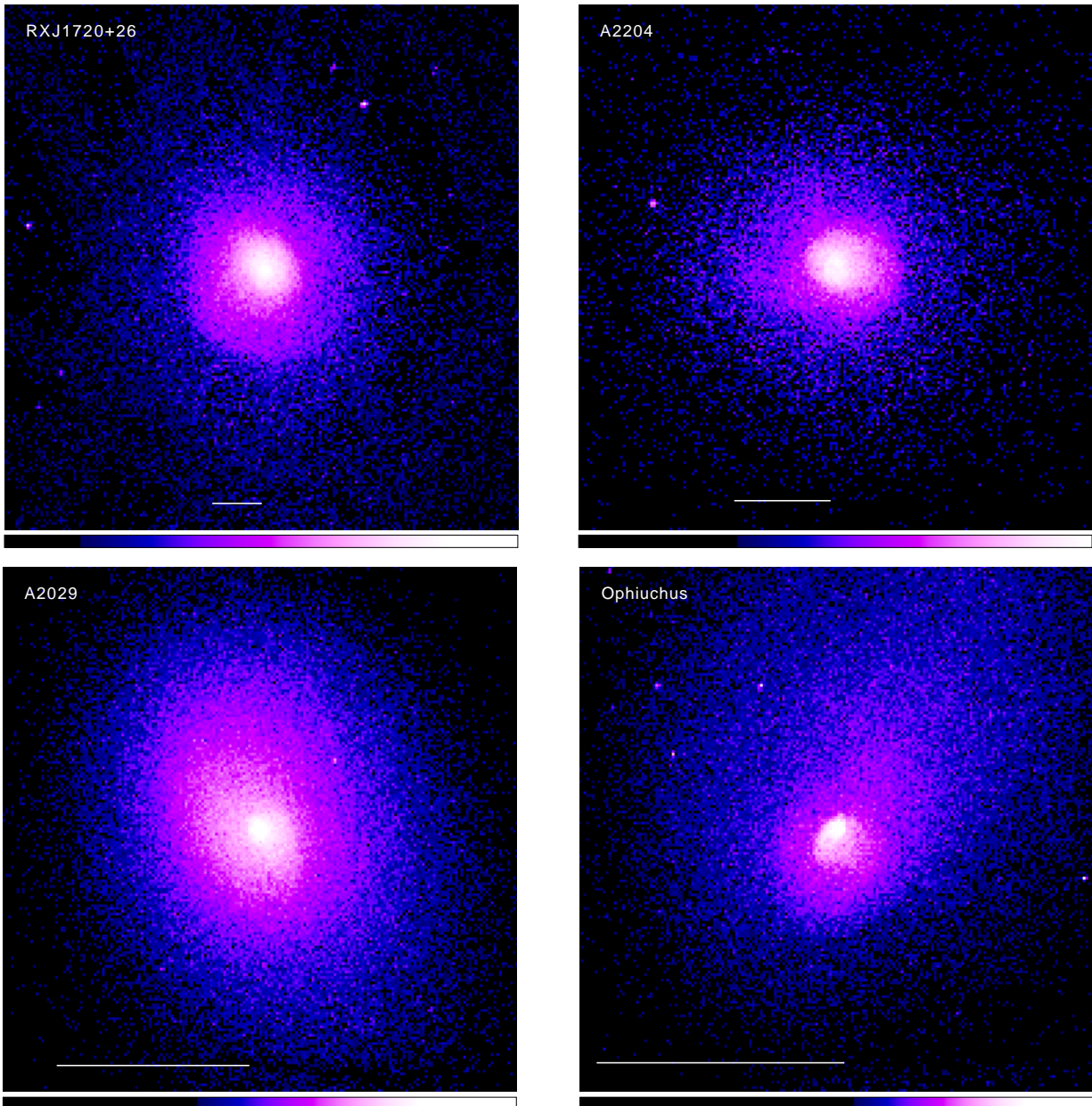


FIG. 1.— Archival *Chandra* X-ray images in a 0.5–4 keV energy band of examples of real clusters exhibiting cold fronts in their cool cores. Horizontal bars are 100 kpc. A2029 (analyzed by Clarke et al. 2004) is among the most relaxed clusters known; it exhibits 2 edges in a spiral pattern at  $r \sim 7$  and 20 kpc (between white and pink and between light and dark pink), and possibly another one at smaller scale. RXJ1720+26 exhibits a large,  $r \approx 250$  kpc edge (pink - blue), while A2204 shows a spiral pattern consisting of at least two edges at 20 and 70 kpc (white - pink, pink - blue). Ophiuchus has some evidence in the outskirts of a recent merger. It shows three edges on scales  $r \sim 3$  kpc, 8 kpc and 40 kpc (white - pink, white - darker pink, blue - darker blue).

potential well and cause gas sloshing and cold fronts. On the other hand, Tittley & Henriksen (2005), using mergers extracted from a cosmological simulation, suggested that cold fronts in the cores can result from oscillations of the dark matter core caused by gravitational disturbance from a merging subcluster. We will see that both of these processes are at work.

The simulations presented in this paper improve on the earlier works in several important respects. First, we achieve much higher resolution, 5–10 kpc within the central  $r < 100$  kpc, sufficient to produce sharp cold fronts and comparable to the resolution of the X-ray observations. Second, we use controlled mergers of idealized symmetric subclusters, spanning a range of merger mass ratios and impact parameters, testing

various dark matter and gas profiles as well as mergers where the smaller subcluster has lost all its gas. This makes it easier to identify physical effects at play and separate them from the effects of random initial conditions in cosmological simulations. Most importantly, we use typical *observed* cluster gas density and temperature profiles as initial conditions, including the observed temperature decline in cluster centers, and do not include radiative cooling. Current cosmological simulations, with or without cooling, cannot reproduce central cool regions of real clusters, even qualitatively. At the same time, the steep gas entropy profile in the center turns out to be the most important condition for the creation of cold fronts, so it is necessary to use realistic gas profiles for such simulations, as we do. We use a Smoothed Particle Hydrodynamics

(SPH) code, which lets us trace individual gas particles during the merger. This opens several possibilities that are uniquely interesting for our study — for example, we can see where the gas in the cold front comes from, whose gas ends up in the center of the final merged cluster, and what is the exact mechanism by which the initially continuous gas distribution evolves into a cold front.

## 2. NUMERICAL METHOD

All our simulations have been accomplished with the parallel PMTree+SPH code GADGET2 (Springel 2005). Cosmological expansion has not been considered, and vacuum boundary conditions have been used. The simulation box size was 300 Mpc. The total mass of the system, consisting of a  $T \sim 10$  keV galaxy cluster and an infalling group-sized substructure, is  $M = 1.7 \times 10^{15} M_\odot$  in all the experiments. The gas mass fraction has been set to  $\Omega_{\text{gas}}/\Omega_{\text{dm}} = 0.04/0.3$ , which is the observed cluster value for  $H_0 = 70 \text{ km s}^{-1} \text{ Mpc}^{-1}$  (e.g., Vikhlinin et al. 2005). This corresponds to a total dark matter (DM) mass  $M_{\text{dm}} \equiv M_0 = 1.5 \times 10^{15} M_\odot$  and a total gas mass  $M_{\text{gas}} = 2 \times 10^{14} M_\odot$ . Our experiments involve  $N = 2 \times 10^7$  particles ( $10^7$  DM particles and  $10^7$  gas particles), which translates into a mass resolution  $m_{\text{dm}} = 1.5 \times 10^8 M_\odot$  and  $m_{\text{gas}} = 2 \times 10^7 M_\odot$ . The gravitational softening length was set to 2 kpc, and SPH quantities are based on the nearest 64 particles. The resulting linear resolution (estimated as the distance to the 64-th neighbor) for our default cluster density profile is 5–10 kpc within  $r = 100$  kpc for the main cluster ( $3''$ – $6''$  at  $z = 0.1$ ), widening to 25 kpc at  $r = 500$  kpc. As we will see below (§6), this is indeed the width of the sharpest features produced by the simulations. Snapshots of the simulations have been saved every 10 Myr.

In order to set up the initial conditions, we model both objects, the main cluster and the subhalo, at  $t = 0$  as spherically symmetric systems in hydrostatic equilibrium. For computational convenience, we use a Hernquist (1990) profile for their DM distribution,

$$\rho_{\text{dm}}(r) = \frac{M_0}{2\pi a^3} \frac{1}{r/a(1+r/a)^3}, \quad (1)$$

where  $M_0$  and  $a$  are the mass and scale length of the DM halo. For the gas temperature, we use a phenomenological formula

$$T(r) = \frac{T_0}{1+r/a} \frac{c+r/a_c}{1+r/a_c}, \quad (2)$$

where  $0 < c < 1$  is a free parameter that characterizes the depth of the temperature drop in the cluster center and  $a_c$  is a characteristic radius of that drop. The corresponding gas density can be derived by imposing hydrostatic equilibrium,

$$\rho_{\text{gas}}(r) = \rho_0 \left(1 + \frac{r}{a_c}\right) \left(1 + \frac{r/a_c}{c}\right)^\alpha \left(1 + \frac{r}{a}\right)^\beta, \quad (3)$$

with exponents

$$\alpha \equiv -1 - n \frac{c-1}{c-a/a_c}, \quad \beta \equiv 1 - n \frac{1-a/a_c}{c-a/a_c}. \quad (4)$$

We set  $n = 5$  in order to have a constant baryon fraction at large radii, and compute the value of  $\rho_0$  from the constraint  $M_{\text{gas}}/M_0 = \Omega_{\text{gas}}/\Omega_{\text{dm}}$ . We also will investigate briefly a mass profile without a central cusp in §5.2.

As noted above,  $M_0 = M_1 + M_2 = 1.5 \times 10^{15} M_\odot$ . We chose  $a = 600$  kpc,  $c = 0.17$  and  $a_c = 60$  kpc, so that the gas density

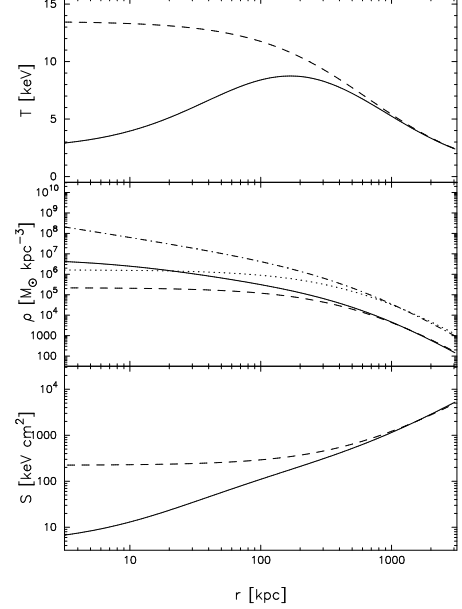


FIG. 2.— Initial conditions for our experiments (from top to bottom, gas temperature, gas and dark matter density and gas entropy). Solid lines show the gas profiles for our ‘standard’ model with  $M_0 = 1.5 \times 10^{15} M_\odot$ ,  $a = 600$  kpc,  $c = 0.17$  and  $a_c = 60$  kpc, while dashed lines correspond to a cluster without a cool core (i.e.  $c = 1$ ). The dark matter density of a Hernquist (1990) sphere is plotted as a dot-dashed line, while the dotted line shows a ‘cored’ dark matter halo described by equation (9).

and temperature profiles of our objects resemble as close as possible those typically observed in massive galaxy clusters at all observable radii, in particular, A2029 (e.g., Vikhlinin et al. 2005). These model profiles are shown in Fig. 2. We will also try a gas profile for the main cluster without a central temperature drop, as well as a subcluster without gas.

We enforce the gas density, temperature and velocity to be single-valued (unlike collisionless dark matter, which may be multi-streaming). The gas density at any point is simply  $\rho_{\text{gas}} = \rho_1 + \rho_2$ . Temperatures and velocities have been weighted by the factor  $w_i = \rho_i/\rho$ , that is,  $T = w_1 T_1 + w_2 T_2$  and  $v = w_1 v_1 + w_2 v_2$ . In the following, we will use ‘‘entropy’’ defined as  $S \equiv T/n^{2/3}$ , where  $n = \rho_{\text{gas}}/\mu m_p$ .

Several experiments have been performed to investigate the effects of the merger mass ratio, impact parameter and energy of the encounter. The mass ratio is defined as

$$R \equiv M_2/M_1, \quad (5)$$

so that  $M_1 = M_0/(1+R)$  and  $M_2 = M_0 R/(1+R)$ . In the following,  $M_1$  and  $M_2$  denote the masses of the infalling satellite and the main cluster, respectively (i.e.  $R \geq 1$ ). In order to scale the initial profiles for various mass ratios of the subclusters, we held  $M/a^3$ ,  $c$  and  $a_c/a$  constant.

Both objects start at a separation  $d = 3$  Mpc, moving towards each other with an initial impact parameter  $b$ . The total kinetic energy of the system is set to a fraction  $0 \leq K \leq 1$  of its potential energy, approximating the objects as point masses,

$$E \approx (K-1) \frac{GM_1 M_2}{d} = (K-1) \frac{R}{(1+R)^2} \frac{GM_0^2}{d}. \quad (6)$$

Thus, the initial velocities in the reference frame of the center of mass are set to

$$v_1 = \frac{R\sqrt{2K}}{1+R} \sqrt{\frac{GM_0}{d}}; \quad v_2 = \frac{\sqrt{2K}}{1+R} \sqrt{\frac{GM_0}{d}} \quad (7)$$

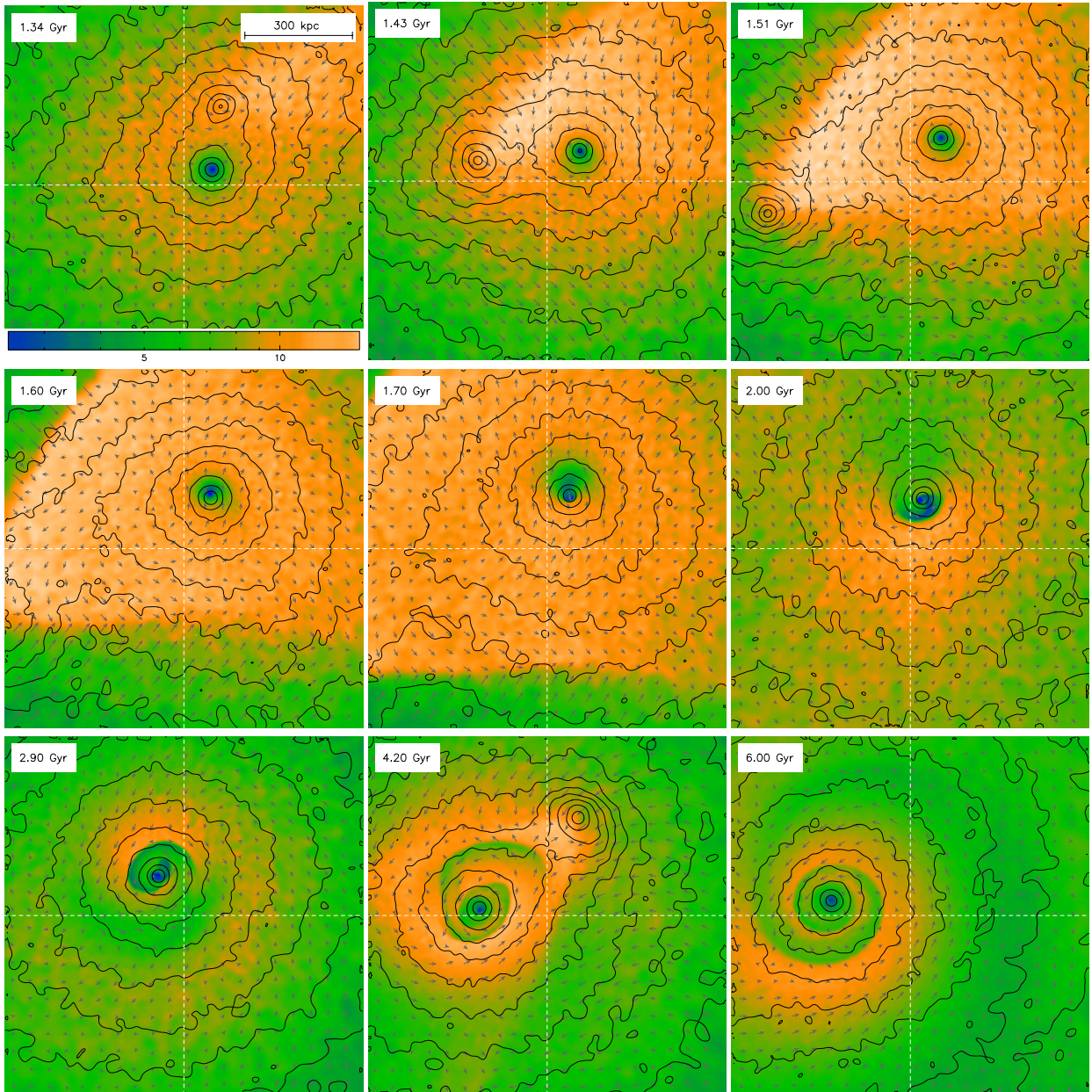


FIG. 3.— Evolution of the cold front induced by a purely dark matter satellite. Parameters of the encounter are  $R = 5$  and  $b = 500$  kpc; the pericenter distance at the first core passage (which occurs at 1.37 Gyr) is  $\sim 150$  kpc. Color maps show the gas temperature (in keV) in a slice in the orbital plane. The temperature scale shown in the top left panel (in keV) is the same for all panels. Arrows represent the gas velocity field w.r.t. the main dark matter density peak (for clarity, the velocity scale is linear at low values, then saturates). Contours are drawn at increments of a factor of 2 in the local dark matter density. The white cross shows the center of mass for the main cluster DM particles (not for the whole system). The panel size is 1 Mpc.

and the total angular momentum is

$$J \approx \frac{R\sqrt{2K}}{(1+R)^2} b M_0 \sqrt{\frac{GM_0}{d}} \quad (8)$$

Different mass ratios ( $R=2, 5, 20$  and  $100$ ) and impact parameters ( $b=0, 500$  and  $1000$  kpc) have been investigated. The initial kinetic energy of the merger has been set to  $K = 1/2$ .

### 3. MERGER WITH A GASLESS SUBCLUSTER

We first consider a simple case (which will also turn out to be the most relevant), in which the infalling substructure is just a DM halo without any gas at all. This situation may arise, for instance, if the satellite lost all its gas due to ram-pressure stripping during an earlier phase of the merger. As

we will see, such a merger does generate sloshing of the cool central gas and multiple cold fronts. Compared to a merger in which both subclusters have gas (considered in the next section), the hydrodynamics in this case is relatively simple and the underlying processes can be identified more easily.

Figure 3 shows the evolution of an encounter with  $R = 5$  and impact parameter  $b = 500$  kpc. While mergers with such massive subclusters may be relatively rare, this choice allows us to see the effects of the disturbance more clearly. For these merger parameters, the first core passage of the satellite takes place at about  $t \approx 1.37$  Gyr from the start of the simulation run, at a distance approximately 150 kpc from the minimum of the gravitational potential. Different values of  $R$  and  $b$  lead to different orbits, with different time and length scales. The extent and intensity of the induced sloshing and subsequent

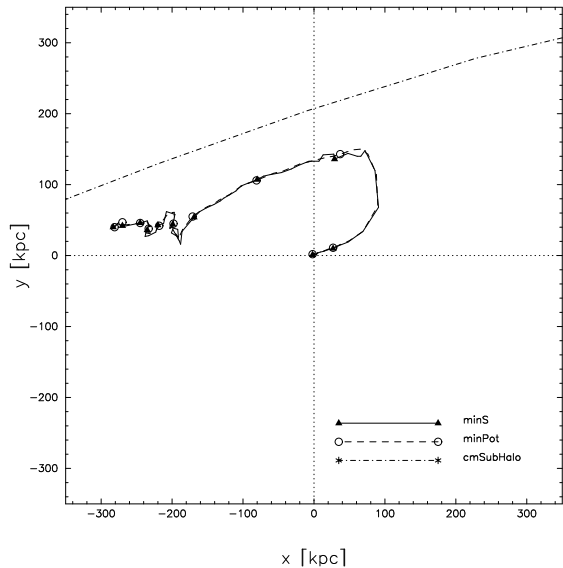


FIG. 4.— Trajectories in the merger plane of the main cluster’s DM peak (circles on dashed line), its gas peak (entropy minimum; triangles on solid line) and the subhalo DM centroid (dotted line) in the reference frame of the *main cluster* mass, for the DM-only subcluster merger. Symbols are spaced by 1 Gyr; the subhalo flyby occurs between 1–2 Gyr. (The DM peak relaxes to a position offset from its initial position in part because the subcluster loses its mass predominantly on one side of the cluster, which shifts the center of mass of the main cluster particles from that of the whole system.)

cold fronts vary, but the qualitative behavior is similar. The cool gas peak is first displaced from the DM peak (around  $t = 1.6$  Gyr in Fig. 3), then falls back and starts sloshing in the minimum of the gravitational potential, generating cool edges. For  $b > 0$ , these edges create a characteristic long-lived spiral structure. We will now look into each of these steps in detail.

### 3.1. Initial gas-DM displacement

There are two independent effects acting simultaneously to provide initial separation of the cool gas from the DM peak during the subcluster flyby. For the DM-only subcluster considered here, the more important effect is the gravitational disturbance that the subhalo creates around the moment of the core passage. It causes the density peak of the main cluster (DM and gas together) to swing along a trajectory shown in Fig. 4 relative to the center of mass of the main cluster, and consequently, relative to the matter and gas surrounding the peak (that is, the matter approximately outside the distance of the closest encounter, 150 kpc, which, for the most part, does not participate in this swinging motion). The gas and DM peaks feel the same gravity force and start moving together toward the subcluster ( $t < 1.4$  Gyr in Figs. 3 and 4). However, after the core passage, the direction of this motion quickly changes. For the gas peak, this leads to a change of sign of the ram-pressure force — compare the gas velocity field outside the cool core in Fig. 3, at 1.43 Gyr and 1.6 Gyr, as well as the gas velocity profiles in Fig. 5 (solid lines). Between these snapshots, the gas velocity around the core changes direction from downward ( $v_y \approx -200$  km s $^{-1}$ ) to upward (+200 km s $^{-1}$ ; hereafter we will refer to the  $y > 0$  and  $y < 0$  directions as “upward” and “downward”, respectively). As a result, the cool gas core, previously compressed by ram pressure from above, shoots up from the potential minimum in a kind of “ram-pressure slingshot” (proposed by Hallman & Markevitch 2004 for a cold front in A168). We will see this effect

more clearly in simulations where the subcluster has gas (§4).

There is another mechanism contributing to the initial gas displacement. Although the subcluster does not have any gas, it drags some of the main cluster’s ICM in a trailing Bondi-Hoyle wake (see e.g. Sakelliou 2000). The subcluster is supersonic at core passage ( $M \simeq 2$ ), but the ICM disturbance that it creates is sonic and the gas density is continuous, unlike that in a shock. This wake will become a weak shock after the core passage, when it starts propagating outwards along the declining density profile. For the off-center merger considered here, this wake transfers some angular momentum from the DM satellite to the ICM, resulting in large-scale rotation of the gas around the main cluster peak.

When this disturbance reaches the central parts of the cluster, it acts to push the cold gas core out of equilibrium. The thermal pressure profile along the vertical line passing through the DM peak is shown in Fig. 6 for different times around core passage. Before the wake reaches the center, one can see the excess pressure from the wake above the cool core (at  $y \approx +200$  kpc for  $t = 1.39$  Gyr). The pressure difference changes sign as the wake passes the core, so that at  $t = 1.5$  Gyr, the pressure below the core (at  $y \approx -100$  kpc) is higher. This is analogous to the sound wave disturbance proposed by Churazov et al. (2003) and Fujita et al. (2004) as a cause of the initial core displacement. This change of the gas pressure difference occurs at approximately the same time as the ram-pressure slingshot described above. The two effects combine to displace the cool gas peak upward (in the  $y > 0$  direction) from the DM peak by about 15 kpc at  $t \simeq 1.6$  Gyr (Fig. 5), while the outlying core gas is displaced to greater distances. (Note that because there is also a gas velocity change across the wake, the two effects are not entirely independent.) Neither the passage of the wake through the core, nor the motion of the core, create any sharp temperature discontinuities until  $t \approx 1.7$  Gyr (Fig. 5), by which time the subcluster has moved 1 Mpc away from the main peak.

### 3.2. Onset of gas sloshing

After the cool gas peak has been displaced from the potential minimum and the displacing force has diminished, the gas starts falling back toward the center. The details of how this happens can be seen in Fig. 7, which shows a zoomed-in view of the gas temperature and velocity field in the core at several interesting moments. The outermost part of the displaced cool gas expands adiabatically as it is carried further out by the upward flow of the surrounding gas (the orange plume above the center in the 1.6–1.7 Gyr panels of Fig. 7). However, in a process not unlike the onset of a Rayleigh-Taylor (RT) instability, the densest, coolest gas quickly starts sinking towards the minimum of the gravitational potential, against ram pressure from the upward flow of the surrounding gas. This is seen most clearly in the 1.6 Gyr and 1.8 Gyr snapshots. At 1.6 Gyr, the cool gas peak starts to flow downward toward the DM center for the first time. By  $t = 1.7$  Gyr, the cool gas has overshot the center and, subjected to ram pressure from the gas on the opposite (downward) side of the DM center still moving upward, spreads into a characteristic mushroom structure, behind which the cool gas continues to flow downward. At 1.8 Gyr, a new RT tongue develops on the inner side of the first mushroom head — the densest, lowest-entropy gas separates and again starts flowing back toward the potential minimum. Meanwhile, the rest of the gas in the mushroom head, and the gas with still higher entropy that by now has started to flow in from above (downward arrows in the or-

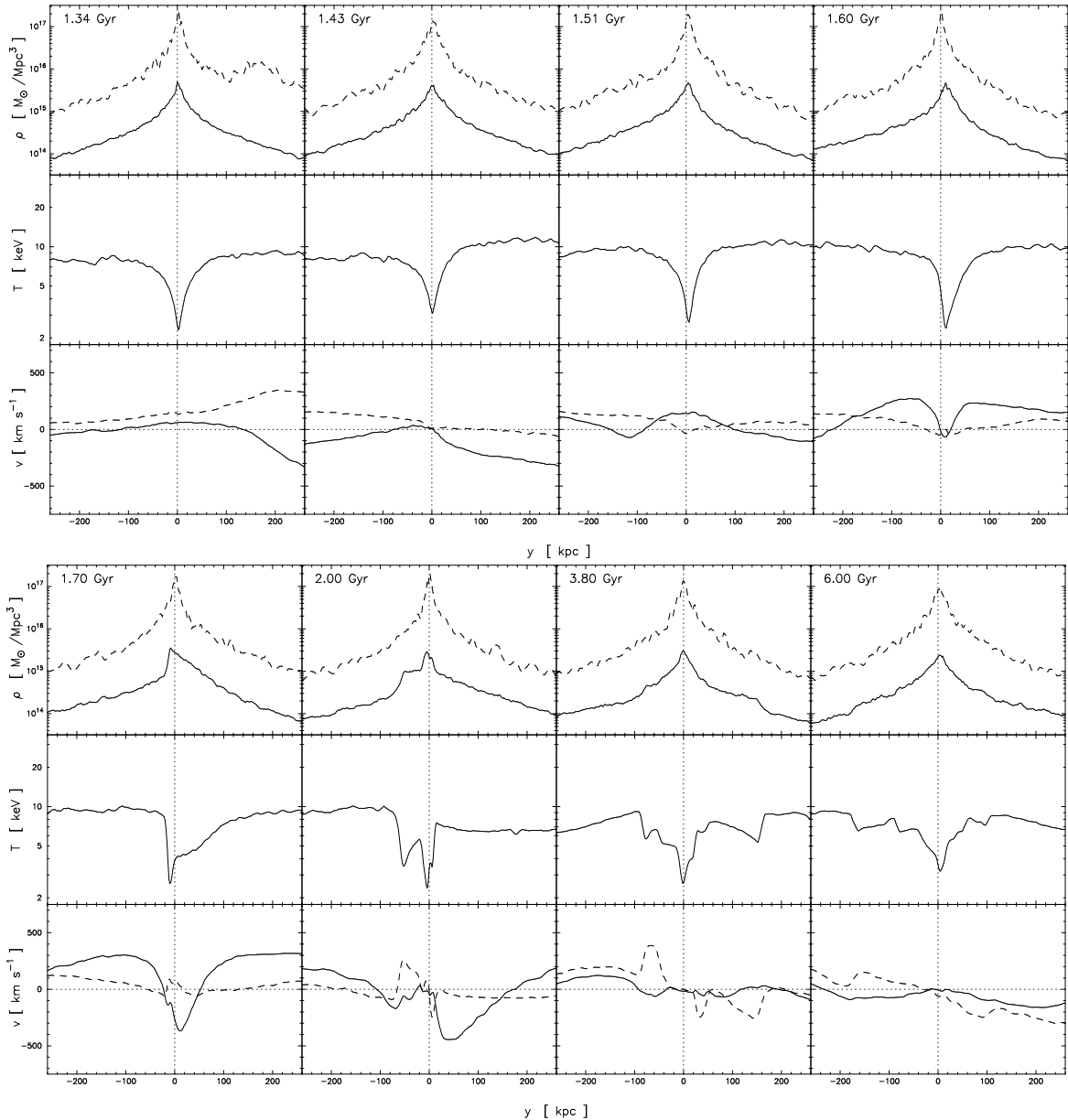


FIG. 5.— Profiles of the DM and gas density, gas temperature, and gas velocity, for the DM-only subcluster run (see Figs. 3 and 7). The quantities have been computed along a vertical line through the DM peak of the main cluster, which is also the frame of reference ( $y = 0$ ,  $v = 0$ ). Solid and dashed lines in the top panels represent gas and DM density, respectively. Solid lines in the velocity panels show the gas velocity along the  $y$ -axis, while dashed lines are used to plot the horizontal component.

ange area in the 1.8 Gyr panel), continues to move outwards, expanding adiabatically as it moves into the lower-pressure regions of the cluster. A snapshot later (1.9 Gyr panel), the coolest gas on its way in (up) encounters ram pressure from the hotter gas that by now has a significant downward velocity, and again develops a classic mushroom structure seen in many hydrodynamic simulations (e.g., Heinz et al. 2003; Takizawa 2005). The stem of the mushroom is the forward flow of the cool gas and the head is where it is slowed by ambient ram pressure and spread sideways, creating characteristic eddies in the velocity field.

Every time the velocity of the densest, lowest-entropy gas is reversed w.r.t. that of the outer, higher-entropy gas in the course of the above RT-like process, the gas parcels with different entropies are quickly brought into contact, creating a cold front. The emergence of these discontinuities (at least

at the resolution of our simulations) is clearly seen in the gas density and temperature cross-sections shown in Fig. 5. We will discuss the precise mechanism by which the discontinuities arise in §7.4.

As we see, immediately after the disturbance from the subcluster flyby, the cool central gas starts sloshing in the minimum of the gravitational potential, creating edge-like discontinuities on progressively smaller linear scales at each new passage through the center. Sloshing of the densest gas that is closest to the center occurs with a smaller period and amplitude than that of the gas initially at greater radii. Note that the oscillation of the DM peak caused by the subcluster flyby has a much longer period (Fig. 4), of order 1 Gyr, than the 0.1 Gyr timescale of gas sloshing. Indeed, as seen in Fig. 7, the DM distribution in the core stays centrally symmetric, while the gas sloshes back and forth in its potential well. This is con-

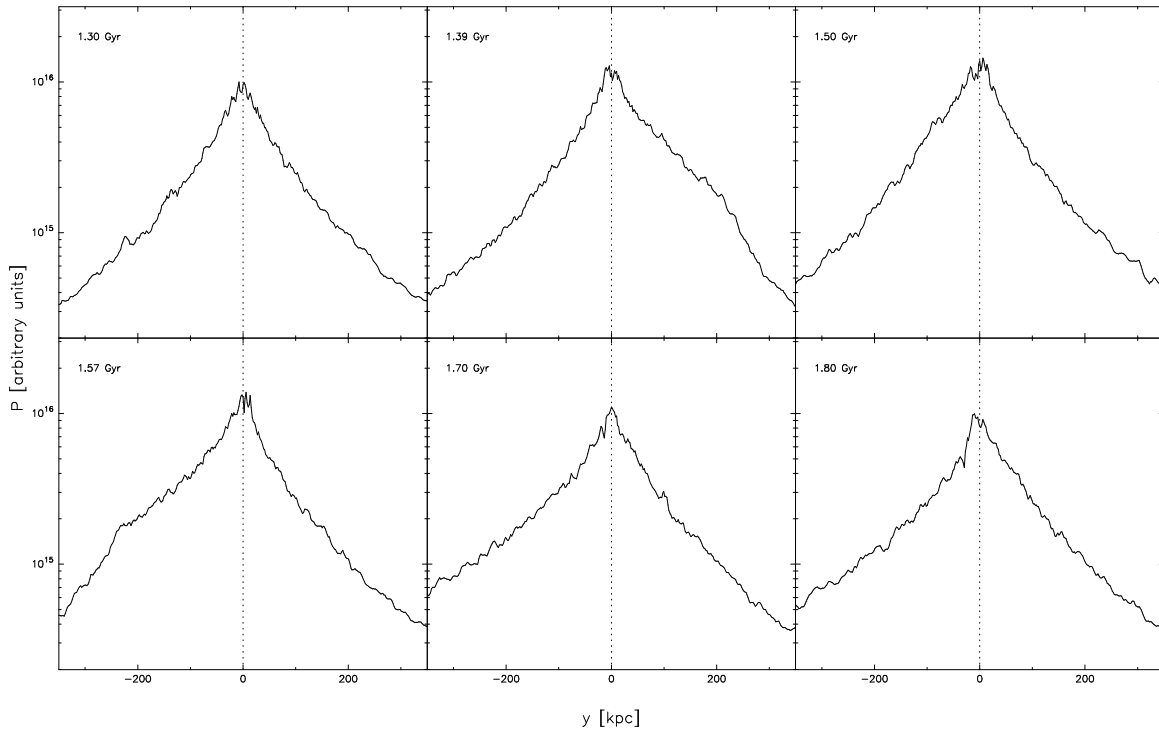


FIG. 6.— Gas pressure along a vertical line through the DM peak, for the DM-only subcluster run, showing the passage of a wake created by the subcluster.

trary to the picture proposed by Tittley & Henriksen (2005) (based on lower-resolution simulations) where the DM peak oscillates back and forth and drags the gas peak along, exposing it to ram pressure. The DM peak motion is indeed one of the two causes of the initial DM-gas decoupling (as discussed above in §3.1), and in the long term, the DM oscillations should continue to feed kinetic energy to the sloshing gas. However, sloshing itself in our simulations is a hydrodynamic effect in a quasi-static central gravitational potential.

### 3.3. The spiral structure

As mentioned above, the off-center flyby of the subcluster transfers angular momentum to the gas near the core via the gas wake. When the cool gas is displaced from the center for the first time, it acquires angular momentum from the gas in the wake and does not fall back radially. As a result, the subsequent cold fronts are not exactly concentric (e.g., the 1.9–2.1 Gyr panels in Fig. 7) but combine into a spiral pattern. Initially, this spiral pattern does not represent any coherent spiraling motion — each edge is an independent structure. In fact, the gas on the opposite ends of each edge flows in the opposite directions. However, as the time goes by and the linear scale of the structure grows, most clockwise motion (i.e., that against the average angular momentum of the outer gas) subsides and the “mushrooms” become more and more lopsided (compare the 1.9 Gyr and 2.9 Gyr panels in Fig. 7). On large scales, the spiral does indeed become a largely coherent spiraling-in of cool gas — the mushroom stems, through which the low-entropy gas flows toward the mushroom cap, shift more and more to the edge of the cap. In the inner regions of the “spiral”, there are still parts flowing in the opposite direction (e.g., at 2.9 Gyr).

Meanwhile, the satellite proceeds on its orbit, reaching apocenter at  $t \approx 2.7$  Gyr and  $r \approx 1.7$  Mpc, and falling back to the core at  $t \approx 4$  Gyr (Fig. 3). During all this time, cold fronts in the core are the only visible trace of the encounter.

The density and temperature contrasts across the cold fronts decrease from a factor of 3 at  $t = 1.7$  Gyr to about a factor of 2 at  $t = 2$  Gyr and  $\sim 1.5$  at  $t = 3.8$  Gyr. The cold fronts generated by the first flyby of the dark matter satellite survive its second passage, which generates new sloshing in the inner part (although less significant, because the satellite has lost some of its mass). Temperature and density jumps at a 20% level remaining from the first encounter are still seen even at  $t = 6$  Gyr, almost 5 Gyr after that encounter (this is, of course, academic, since any real cluster will probably experience a few more mergers during this period).

One interesting question that may arise from looking at the evolution of the spiral temperature structure (Figs. 3 and 7) is how the small initial displacement of the central cool gas apparently succeeds in spreading this low-entropy gas out to large radii against convective stability in the radially increasing entropy profile. In fact, this is not the case. Figure 8 shows the ratio of the radial distances of the gas particles at present to their initial distances from the center of the undisturbed cluster. All cool structures are indeed comprised of gas that has moved away from the center. However, the amplitude of the radial change is diminishing with time. At 2 Gyr, sloshing displaces the gas along the radial coordinate by up to a factor of 3, while at 6 Gyr it is not more than a factor of 1.5. That is, as expected, the gas that initially splashes out to large distances eventually settles back in the center. The cool gas that forms the large-scale cold fronts at later stages has not come all the way from the center, but from only slightly smaller radii (although possibly from the opposite side of the cluster). It expanded adiabatically, which enhanced the temperature contrast. While Figs. 3 and 7 show that each cold front indeed starts near the center and expands continuously, the gas at the front is not the same at every moment. As seen most clearly in the 1.9–2.1 Gyr panels of Fig. 7, there is circulation inside the cold front, in which the lowest-entropy gas

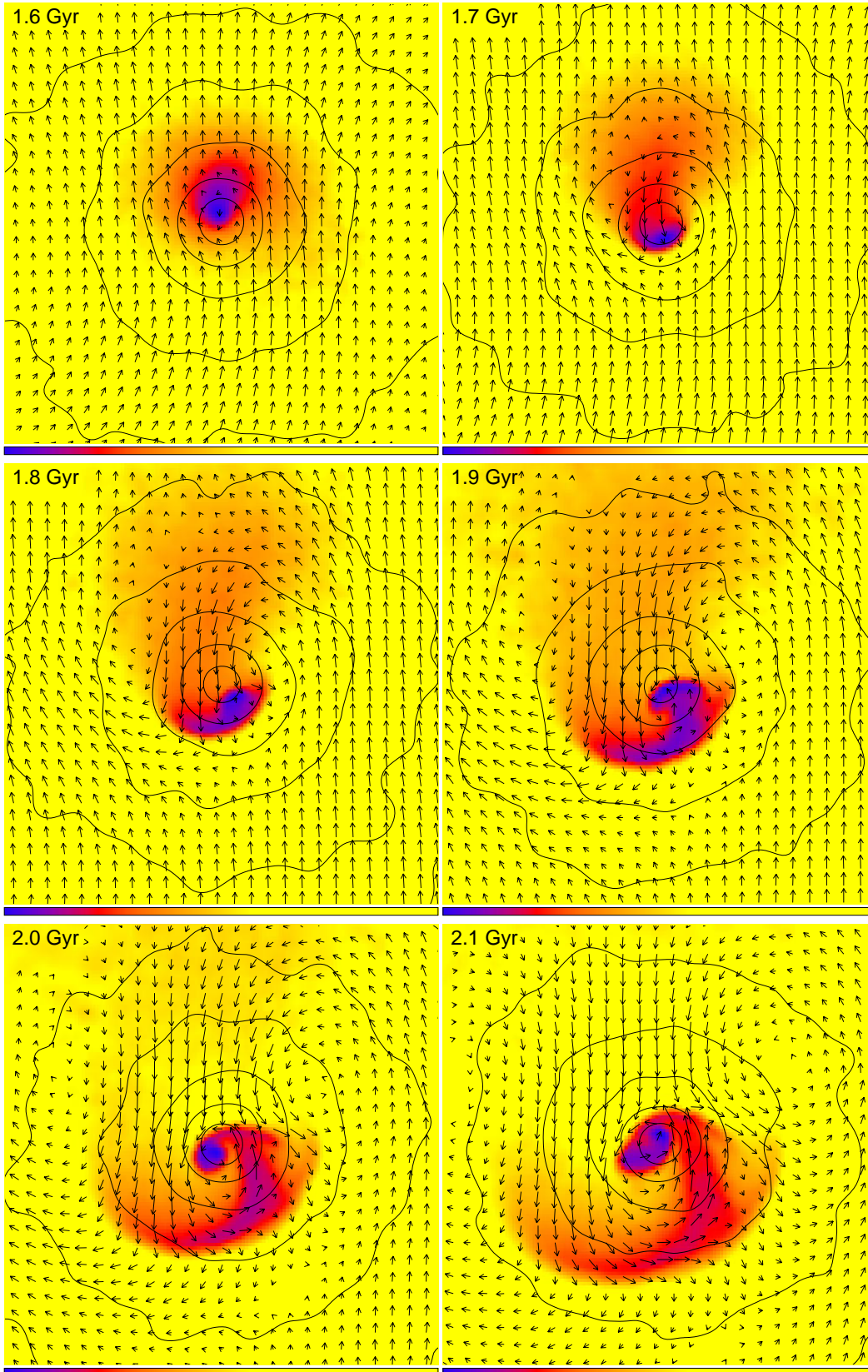


FIG. 7.— Zoomed-in gas temperature slices (color; blue is 2 keV, yellow is 7–9 keV) with DM density contours overlaid (log-spaced by factor of 2), for the pure-DM subcluster run shown in Fig. 3. The size of the panels is 0.25 Mpc, except 3.8 Gyr which is 0.33 Mpc. The gas velocity field, relative to the DM peak, is shown by arrows (the longest arrows are  $500 \text{ km s}^{-1}$  and the scale is linear;  $v < 30 \text{ km s}^{-1}$  are not shown). For comparison, the sound speed in the 7–9 keV gas is  $1300\text{--}1500 \text{ km s}^{-1}$ . Time labels are the same as in Fig. 3.

continuously flows back from the front toward the center. It

is replaced at the front by higher-entropy gas that arrives later



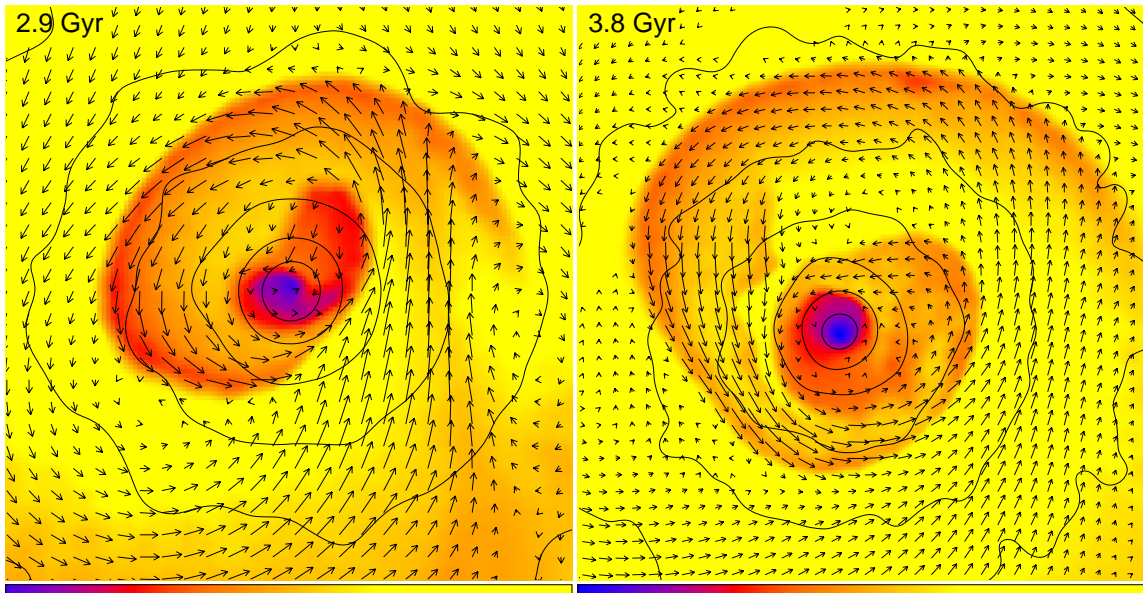


Fig. 7. — continued

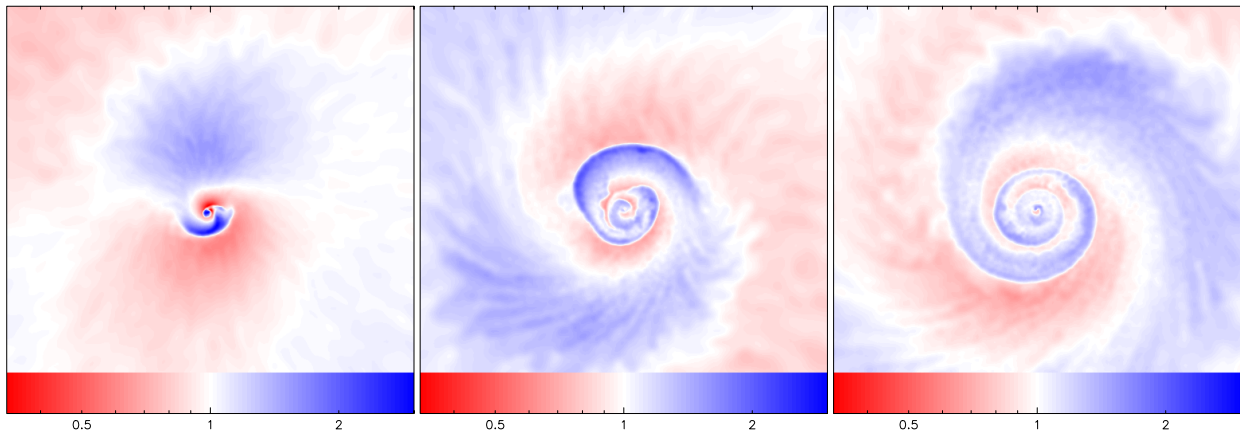


FIG. 8.— The relative radial displacement of the gas particles,  $r/r_0$ , where  $r_0$  is the initial radial distance of the particle, for  $t = 2.0, 3.8, 6.0$  Gyr, for the DM-only subcluster run (the same slices as shown in Fig. 3). Both  $r$  and  $r_0$  are relative to the DM peak of the main subcluster at the corresponding time. Panels are 1 Mpc in size, centered on the DM peak.

and whose origin traces back to greater radial distances. Finally, the oscillation of the DM peak on a Gyr timescale relative to the bulk of the cluster gas also contributes to widening the spiral pattern.

We note here that our conclusion about the longevity of the spiral structure may be affected by two numeric effects. As will be discussed in §6, the finite resolution and the artificial viscosity employed in the SPH code suppress small-scale turbulence that might disrupt the sharp features and mix the gas with different entropies (although this is not necessarily a problem, because viscosity in real clusters is not known and may be comparable). It also injects entropy into the gas wherever there is velocity shear, including at cold fronts. This entropy increase may make it slightly more difficult for that gas to sink back to the center. However, the origin and the near-term evolution of the cold fronts should be reproduced qualitatively correctly.

#### 4. THE EFFECT OF SUBCLUSTER GAS

If the infalling subcluster has retained its gas, the picture is very different from that described in §3. Figure 9 shows a simulated encounter with the same parameters as the one

described in the previous sections ( $R = 5$  and  $b = 500$  kpc), but now the infalling satellite has its own gas component. The most important difference is that the gas of the subcluster now displaces the gas of the main cluster, creating a shock front — a region of high-density, hot gas moving with the same velocity ( $M \approx 2$  at core passage in our fiducial setup), which should be compared to a more subtle sonic wake that accompanied the DM-only subcluster. The shock and the gas stripped from the subcluster are now the dominant agents disturbing the gas at the main core, much more significant than the slow orbital motion of the main DM peak. If the merger is head-on, they can sweep the cool gas from the main cluster completely. As long as the merger is off-center and the central gas survives the shock passage, the gas starts sloshing in a process qualitatively similar to that seen in the DM-only subcluster run.

The 1.3–1.5 Gyr panels in Fig. 9, as well as the gas density and velocity profiles through the center plotted in Fig. 10, show again the effect of a ram-pressure slingshot. To illustrate it more clearly, Fig. 11 shows profiles of the quantity which approximately represents ram pressure on the upper-right side of the main core, at several interesting moments of time. At core passage ( $t = 1.35$  Gyr), the ram pressure on the cool den-

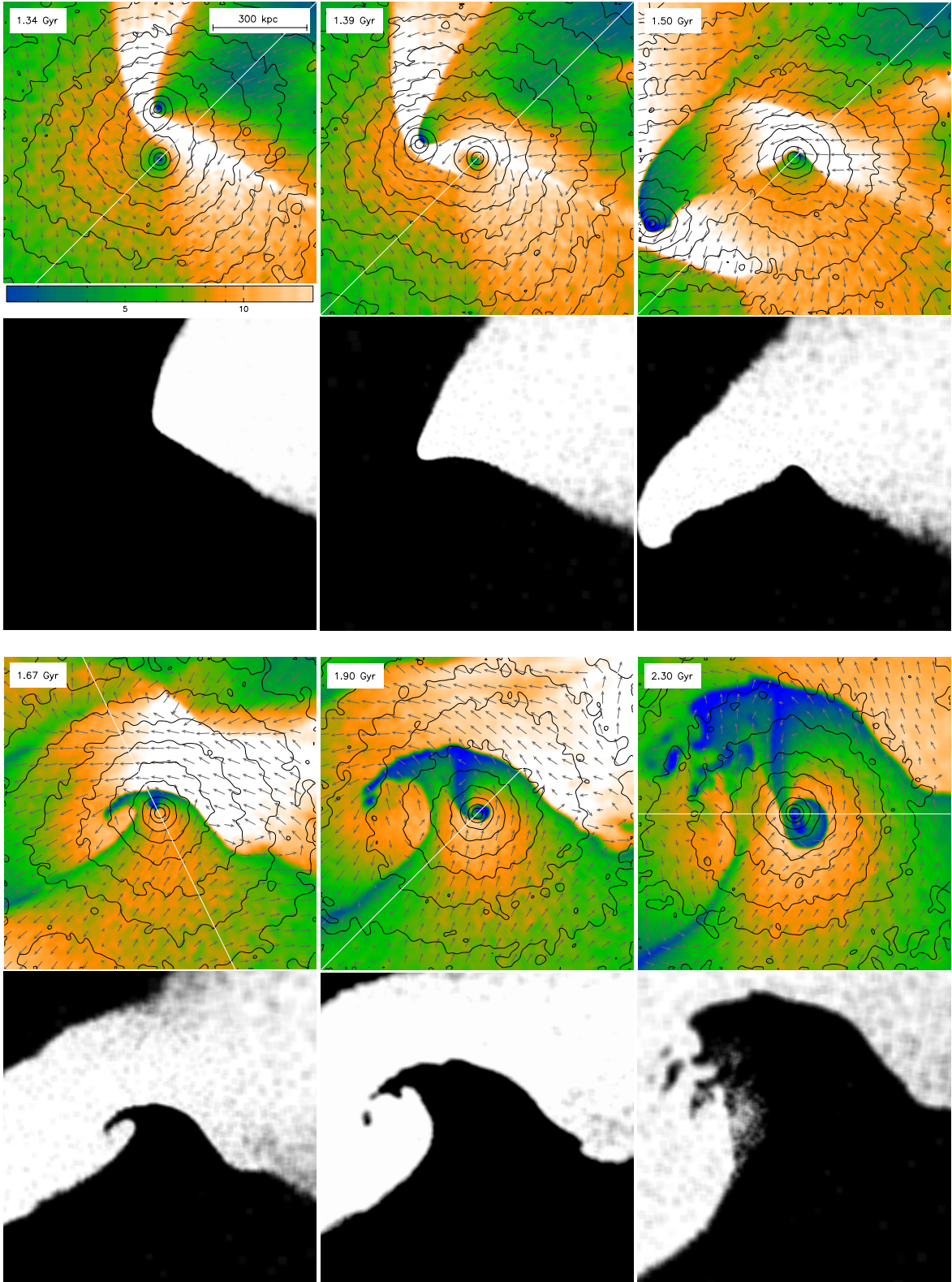


FIG. 9.— Temperature slices for the same encounter as in Fig. 3 ( $R = 5$ ,  $b = 500$  kpc), but now the satellite that has its own gas component. A black-and-white plot under each image shows the fraction of particles initially belonging to the two subclusters (black is main cluster, white is subcluster). The panel size is 1 Mpc. The profiles in Fig. 10 are derived along the white lines in these temperature plots.

sity peak is at its maximum; it is strong enough to compress and displace much of the main core gas to the lower-left from the DM peak (this displacement can be seen in the 1.39 Gyr panel in Fig. 9). As soon as the subcluster moves away, ram pressure drops very quickly (although not monotonically, be-

cause initially it is exerted by the shocked gas and then by the stripped subcluster gas, as can be understood from Fig. 11). This causes the gas in the main core to rebound and overshoot the DM peak. Around  $t = 1.5 - 1.6$  Gyr, there is an interesting additional effect — the rebounding dense core sticks out

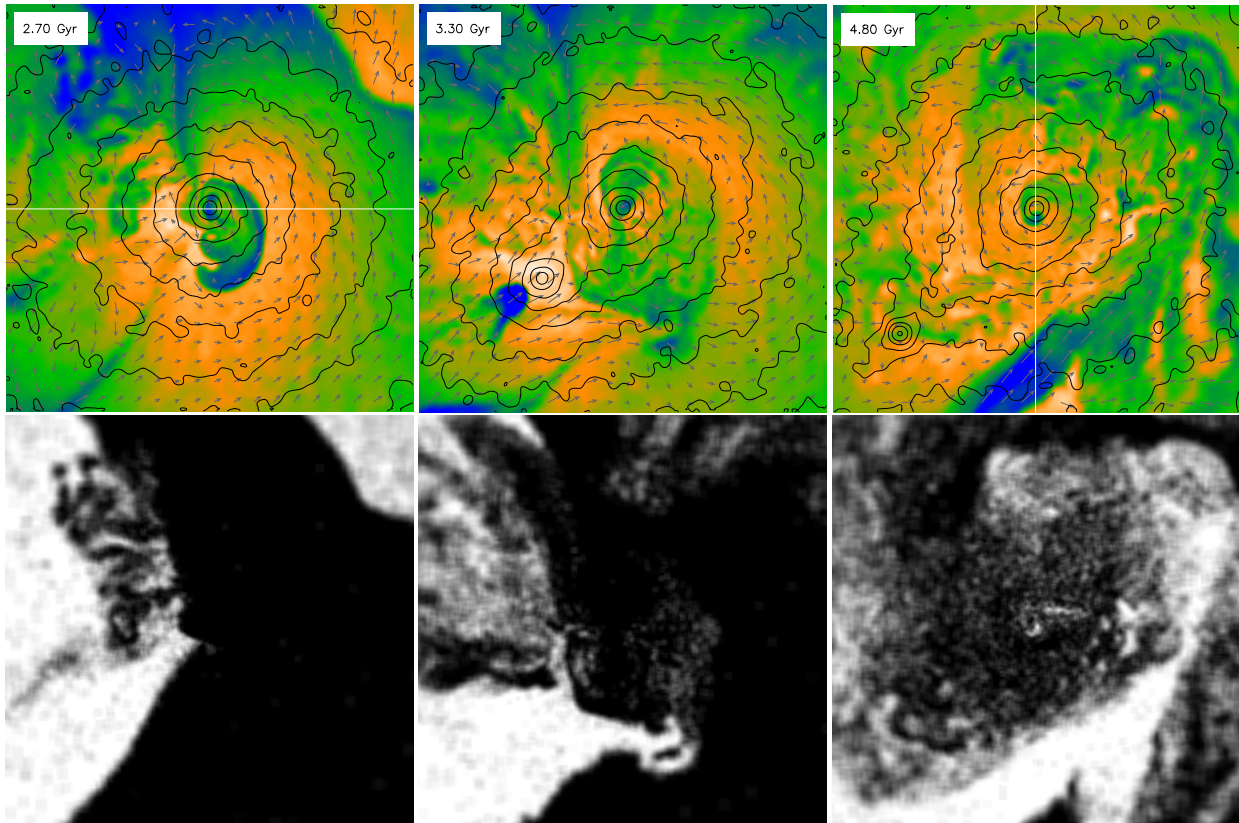


Fig. 9. — continued

into the flow of the subcluster gas (see the 1.5 Gyr gas fraction panel in Fig. 9), making the subcluster ICM flow around it. This creates an “airplane wing” effect, additionally lifting this gas up.

The first sharp cold front (Fig. 10) forms at  $t \approx 1.5$  Gyr as a result of this rebound motion. Compared to the DM-only subcluster run, the cold front forms earlier and on the opposite side from the core — because the initial gas-DM displacement is now caused by ram pressure from the subcluster, not by the change in the direction of motion of the main DM core as it was in §3.1. This front separates the main cluster and the subcluster ICM. The tangential flow of the subcluster gas along its surface creates an eddy seen in the 1.67–1.9 Gyr panels of Fig. 9. Note that not just the cool gas from the core, but the bulk of the main cluster gas, initially pushed to the south by the subcluster flyby, rebounds and takes part in the upward flow. However, the densest, coolest gas quickly develops a RT-like tongue (the 1.67 Gyr panel in Fig. 9) and starts flowing back into the potential minimum (such cool filaments behind cold fronts were also seen in the simulations by Mathis et al. 2005). From this moment on, the picture is qualitatively similar to our DM-only subcluster run (§3). This cool gas reaches the potential minimum and starts sloshing in it, generating mushroom-head cold fronts and RT tongues on smaller and smaller scales, similar to Fig. 7. Inside each of these mushroom heads, as well as inside the first “slingshot” cold front, the lowest-entropy gas is constantly flowing toward the DM peak along the RT-like tongues and is replaced at the cold front with the newly arrived, higher-entropy gas, as described in §3.3. This allows the cold fronts to expand outward. Note that the “slingshot” cold front separates gases from the two merging subclusters, while the “sloshing” cold fronts in the center arise entirely within the ICM of the main

cluster, as in §3.

The “slingshot” cold front moves beyond  $r = 500$  kpc approximately 1 Gyr after the core passage (where it still exhibits a factor of  $\sim 2$  density jump). Compared to the DM-only subcluster run, the initial disturbance was much stronger and the sloshing cold fronts evolve much faster. In addition, the velocity field is more chaotic due to the eventual infall of the gas stripped from the subcluster, which destroys most of the central pattern of “sloshing” cold fronts in about 2 Gyr (the 3.3 Gyr panels in Fig. 9).

#### 4.1. Stripping of the subcluster gas

The subcluster gas in the simulation shown in Fig. 9 illustrates a classic ram pressure stripping scenario. As the subcluster falls in for the first time, its outer gas is stripped and forms a comet-shaped tail (1.34–1.5 Gyr gas fraction panels in Fig. 9). At  $t = 1.5$  Gyr, the cool dense gas in the main cluster core presents an obstacle to the smooth supersonic flow of this stripped gas. This gives rise to a second bow shock clearly seen in the 1.5 Gyr panel “in front of” the main core, making the picture symmetric.

The front tip of the gas still remaining in the subcluster core is a sharp cold front caused by ram pressure stripping early in the merger. At core passage, where the infall velocity and the ambient gas density are at their maximum, ram pressure on this remaining gas is so high that the gas is pushed back from the subcluster’s DM peak. At  $t \approx 1.4$  Gyr, our subcluster looks much like the “bullet” in 1E0657–56, which exhibits a shock front, a cold front, and cool gas lagging the DM peak (Markevitch et al. 2002).

As the subcluster moves out, the ram pressure rapidly diminishes, and we again see the effect of the ram-pressure/gravity slingshot, which at  $t = 1.5$  Gyr returns the

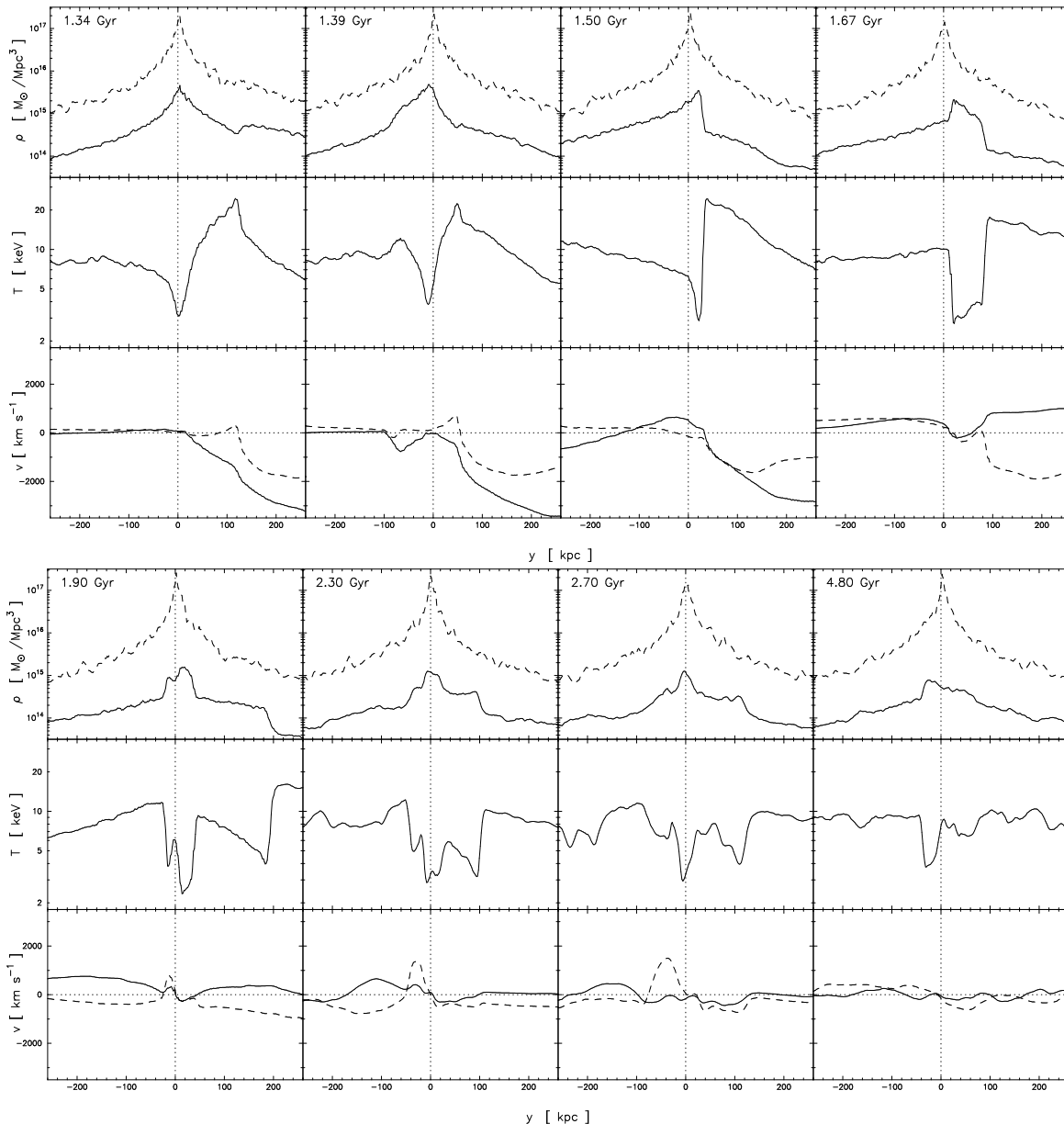


FIG. 10.— Density, temperature and velocity along the white lines in Fig. 9. As in Fig. 5, solid and dashed lines in the top panels represent gas and DM density, respectively; solid and dashed lines in the velocity panels show the components parallel and perpendicular to the  $y$ -axis (white lines in Fig. 9), relative to the DM peak. Note that the velocity scale is much larger than in Fig. 5.

cool gas to the DM peak and later makes it overtake the DM peak, as seen, e.g., in the A168 cluster (Hallman & Markevitch 2004) and in the Mathis et al. (2005) simulations.

Around  $t = 3.4$  Gyr, the subcluster falls in for the second time. By this time it has lost a large fraction of its DM mass and is not able to retain any of its gas after the second core passage. In the 3.3 Gyr panel of Fig. 9, we see how the cool gas peak is completely detached from the DM peak as soon as they enter the dense region of the main cluster. Eventually, this most persistent parcel of cool gas falls to the center of the main cluster, where it starts sloshing in the potential minimum (4.8 Gyr panels in Figs. 9 and 10). By that time, the main cluster’s own cool central gas has escaped from the core. At this stage, the cluster looks relatively relaxed on a large scale (§7.1); the most notable feature is this sloshing cool gas in the center which originally belonged to the infalling subcluster. This curious replacement of the gas in the center does not

occur for all combinations of the merger mass ratios and impact parameters. We should also note that artificial viscosity and the finite resolution of our simulations inhibit small-scale turbulence, which may act to mix the ICM from the two subclusters earlier.

## 5. EXPLORING THE PARAMETER SPACE

### 5.1. Main cluster without cooling flow

For a contact discontinuity at constant pressure, a density and temperature jump by a factor of two corresponds to an entropy ratio of  $2^{5/3} \sim 3$ . The obvious condition for the formation of a cold front is that gases with such different entropies should exist in the cluster in order for a merger to bring them into contact. Clusters with “cooling flows” do have steep radial entropy gradients in the centers which, as we saw above, are sufficient to produce cold fronts when disturbed. However, about 1/3 of the nearby clusters do not have

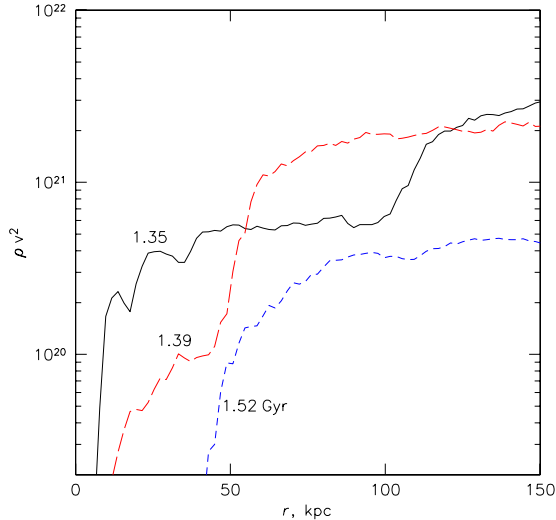


FIG. 11.— Ram pressure exerted on the upper-right side of the main cool gas core during the subcluster fly-by, for the gas run shown in Fig. 9. The quantity shown is the product of the gas density and the square of the radial component of the inflow velocity (relative to the DM peak) along the diagonal line from the DM peak to the upper-right. Units are arbitrary. The distance is from the DM peak, the labels show moments of time. At  $t = 1.35$  Gyr, the pressure on the core is exerted by the shocked main cluster gas; the second bump around  $r = 100$  kpc is the approaching gas stripped from the subcluster (at 1.39 Gyr, it moves to  $r = 50$  kpc). After reaching a maximum around 1.35 Gyr, the ram pressure generally declines rapidly with time, resulting in a slingshot-like rebound of the main cluster gas.

cooling flows, instead exhibiting roughly isothermal flat gas cores. In such clusters, the gas is fairly well fitted by a simple  $\beta$ -model,  $\rho_{\text{gas}} \propto (1 + r^2/r_c^2)^{-3\beta/2}$  with  $r_c \sim 100$  kpc. The gas entropy is still increasing with radius in the cores of such clusters, but much slower than in the cooling flow clusters. It is interesting to see if such low entropy contrast is sufficient to generate sloshing and cold fronts.

We have performed an experiment in which the initial density and temperature profiles for the main object are derived using  $c = 1$  in equation (2), which corresponds to no cool central component. Both DM profiles are kept the same, and the subcluster still possesses a cool core with  $c = 0.17$ . All other merger parameters are also the same. For  $c = 1$  and our fiducial DM profile for the main cluster, the gas temperature and density profiles given by expressions (2) and (3) are similar to a  $\beta$ -model with  $r_c = 115$  kpc. For this profile, the entropy increase by a factor of 3 from its central value is reached at  $r = 560$  kpc, while between  $r = 0$  and  $r_c$ , it increases only by a factor of 1.6. For comparison, for our default cooling flow profile with  $c = 0.17$ , the entropy rises by a factor of 3 already at  $r \sim 70$  kpc.

The results are shown in Fig. 12. The gas core of the main cluster is now easily pushed downward from the DM peak by the ram pressure of the stripped subcluster gas. As this ram pressure diminishes, we see the development of a “slingshot” cold front (2.0 Gyr panel in Fig. 12), similar to that in our simulations with a cool gas peak (compare to the 1.9 Gyr panel in Fig. 9). As before, this cold front is a contact discontinuity between the main cluster and the stripped subcluster gases. With time, it travels beyond  $r = 1$  Mpc, maintaining a density contrast around a factor of 2.

However, no RT instabilities form inside the region delineated by this cold front — there is just not enough entropy contrast for them to develop. So no cool gas is flowing back

to the DM peak and there is no sloshing seen in the main cluster’s core, until the stripped dense, cool central gas from the subcluster falls there several gigayears later. This experiment shows that although the cluster without a steep central entropy decline can produce a large, prominent cold front of the “slingshot” origin in the course of a merger, “sloshing” cold fronts do require a cooling-flow type gas profile.

A cooling flow-like temperature drop is not required, as long as there is an entropy gradient. Ricker & Sarazin (2001) simulated a merger in an isothermal cluster with a cuspy potential, which shows the formation of similar multiple mushroom heads. The specific entropy declines toward the center less steeply than in a cooling flow cluster, hence the linear scale of the resulting sloshing is bigger (note also that this merger involves a gas-containing subcluster, so the initial disturbance was greater).

### 5.2. Main cluster without DM cusp

It is also interesting to see how the shape of the central DM profile affects the generation of cold fronts — in particular, if the DM density cusp,  $\rho_{\text{dm}} \propto r^{-1}$ , in the center of a Navarro, Frenk & White (1995) halo or the Hernquist (1990) profile used here, is a necessary condition. For this, we consider a limiting case where the main cluster DM profile is given by

$$\rho_{\text{dm}}(r) = \frac{3M_0}{4\pi a^3} \frac{1}{(1+r/a)^4}, \quad (9)$$

which features a constant-density core at  $r \ll a$ .

The gas still has a cooling-flow like density peak at the center. While this situation does not seem likely in nature, it is a useful test case. The gas temperature profile is given by equation (2), and the density profile is computed numerically from the hydrostatic equilibrium equation. We have set the free parameters of the model to the values  $M_2 = 1.1 \times 10^{15} M_\odot$ ,  $a = a_c = 300$  kpc and  $c = 0.3$ , so that the initial temperature and density profiles of the ICM are as close as possible to those of the previous experiments in §§ 3-4 (and to those observed in real cooling flow clusters). The subcluster has the same gas and DM profiles as before, and the mass ratio and the impact parameter of the merger are the same as in §§3-4.

Results of this simulation are plotted in Fig. 13. All the salient features observed in a cluster with the cuspy DM profile (§4) are present — a “slingshot” cold front, a RT tongue of low-entropy gas flowing back into the core, and subsequent sloshing of this gas in the core with the creation of non-concentric cold fronts. The notable difference is that the amplitude of this sloshing is wider and its period longer (and therefore the cold fronts are fewer) than in §4, as expected for the weaker gravitational attraction toward the cluster center. Thus, sloshing of the cool, dense central gas and the resulting cold fronts can develop in a wide range of cluster DM profiles, from flat to cuspy.

### 5.3. Subcluster mass ratio

In this and the following section, we investigate which merger mass ratios and impact parameters are more favorable to the formation of cold fronts in the cluster centers.

Encounters with different mass ratios are shown in Fig. 14. All other parameters are set to the same values as in §4, the satellite has its own gas component and the main cluster has both a DM cusp and a cooling flow. Major mergers ( $R = 2$ , top panel) trigger extremely strong perturbations in the ICM of the main cluster. Both “slingshot” and “sloshing” cold fronts

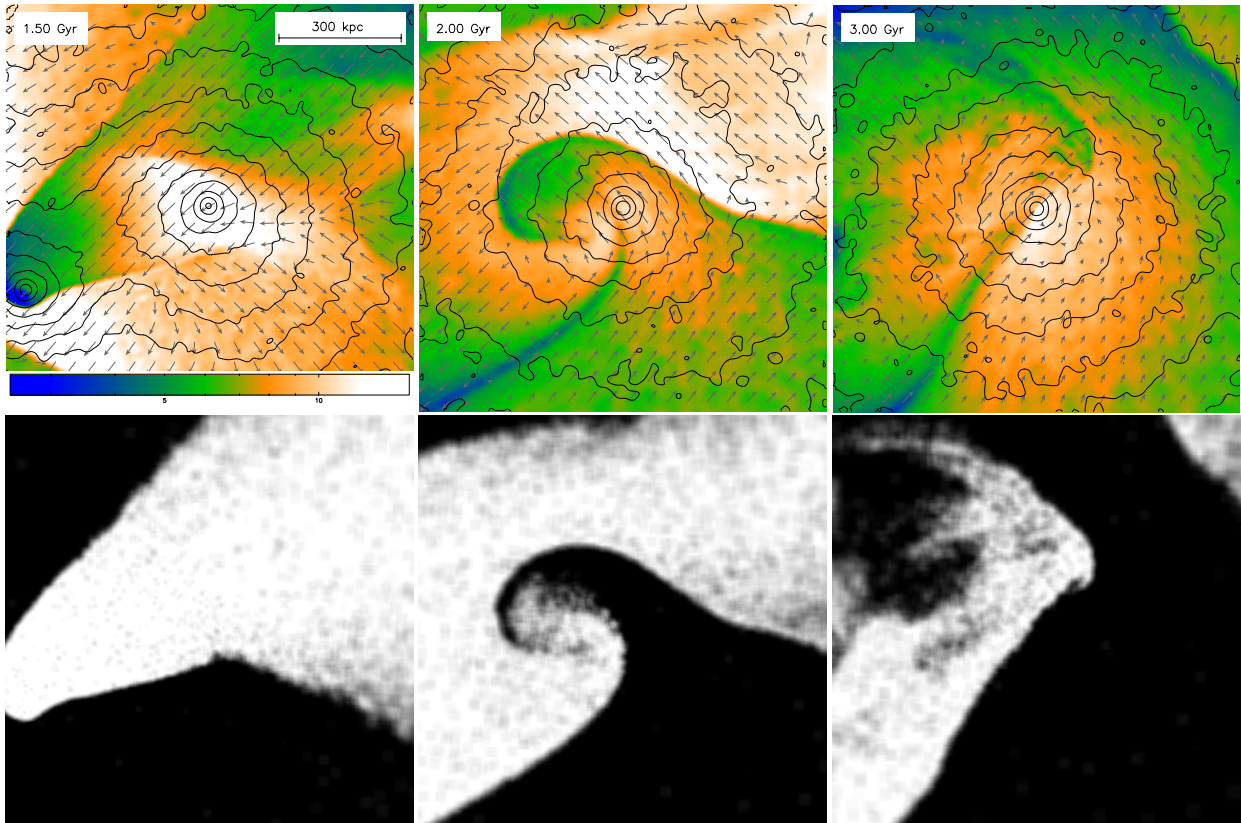


FIG. 12.— Encounter with  $R = 5$ ,  $b = 500$  kpc (as in Fig. 9), but the main cluster has a flat gas density profile without a central temperature drop (see Fig. 2). The satellite, however, still possesses a cool gas core. A plot under each image shows the fraction of particles belonging to the two subclusters. Even though there is no cool gas in the main cluster, its entropy still declines toward the center, and the low-entropy gas still creates a cold front (middle panel), which quickly moves outwards.

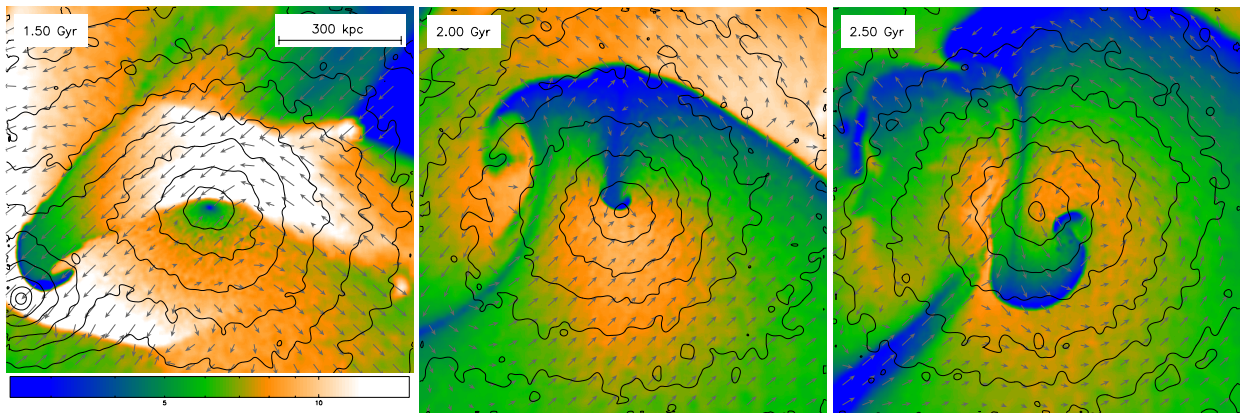


FIG. 13.— Encounter with  $R = 5$ ,  $b = 500$  kpc (as in Fig. 9), but now the DM density profile of the main cluster has a flat central core instead of a cusp (eq. 9), while the gas in both subclusters has cool peaks. The behavior is qualitatively similar to the run with a cuspy DM profile, but the amplitude of sloshing is much larger.

form after the first passage of the satellite, but its second passage about 1.5 Gyr later (for our particular merger parameters) destroys them. There are obvious signatures of merging during most of the process, so the cluster would not look “relaxed” until long after the merger. When the system finally settles down into equilibrium, sharp discontinuities in the core have been erased by shock heating and vigorous turbulence.

More modest mergers with  $R = 20 - 100$  (middle and lower panels in Fig. 14) produce longer-lived cold fronts in the main core. Such small subclusters, merging with this particular impact parameter ( $b = 500$  kpc), do not cause a complete detachment of the cool gas peak from the DM peak, contrary to

the  $R = 2$  case above and our default simulation with  $R = 5$ . There is a weak slingshot front, but with little (for  $R = 20$ ) or no (for  $R = 100$ ) RT-like filament of cool gas flowing from the front inward — the lowest-entropy gas has never left the center. The pressure disturbance is still sufficient to displace the coolest gas and cause its sloshing. Thus, during mergers with the smallest subclusters, the behavior of the gas in the center of the main cluster initially looks almost like that in a pure-DM subcluster run (§3). A big difference, however, is the cool gas from the subcluster that is completely stripped during the first passage. This gas quickly falls into the center, causing turbulence and destroying any coherent structure there. This

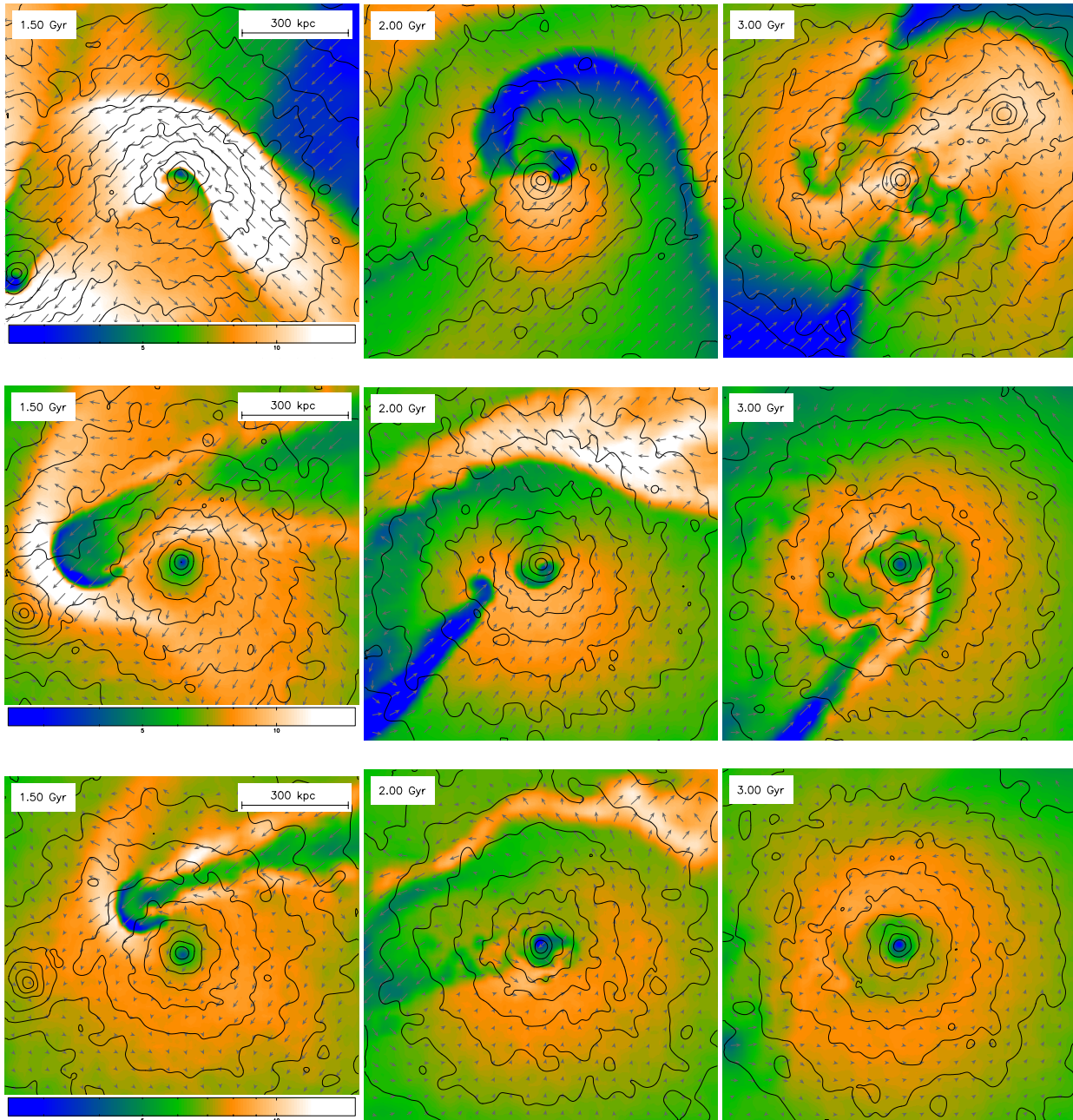


FIG. 14.— Encounters with different mass ratios:  $R = 2$  (top), 20 (middle) and 100 (bottom);  $b = 500$  kpc in all cases. Both subclusters have central DM cusps and cool gas peaks. These simulations have been run at a lower resolution, with  $2 \times 10^6$  (gas + DM) particles.

occurs more quickly for less massive subclusters — about 0.8–1 Gyr after the core passage for the  $R = 20$  merger, but only 0.4 Gyr for the  $R = 100$  merger. In a few gigayears, this gas will relax into a new cool core, and the remaining pure-DM satellite may cause sloshing during subsequent pericenter passages, as in §3.

#### 5.4. Impact parameter of the merger

The generation and survival of cold fronts also depends on the merger impact parameter. In one extreme, a head-on merger with a subcluster containing gas is likely to destroy the central cool core and generate a chaotic velocity field which precludes the formation of any coherent structures (top panel in Fig. 15). The exception is a merger in which the subcluster has such low gas density that it is completely stripped before the DM subcluster passes the main core. This case would

be similar to a head-on merger with a DM-only subcluster, which is a simple symmetric limiting case of the encounter discussed in §3. It generates sloshing and concentric cold fronts at smaller and smaller radii in the main core via processes discussed in detail in that section. The significant difference here would be that the stripped subcluster gas eventually falls into the center and disturbs those fronts.

Encounters with a large impact parameter are more favorable to the formation and survival of the cold fronts in the center. Lower panel in Fig. 15 shows a simulation for  $b = 1$  Mpc. The overall picture is qualitatively similar to our default  $b = 500$  kpc case (Fig. 9). However, the slingshot cold front forms at a greater radius and is more detached from the densest gas in the core, which is never significantly separated from the main DM peak. The low-entropy gas (not quite so

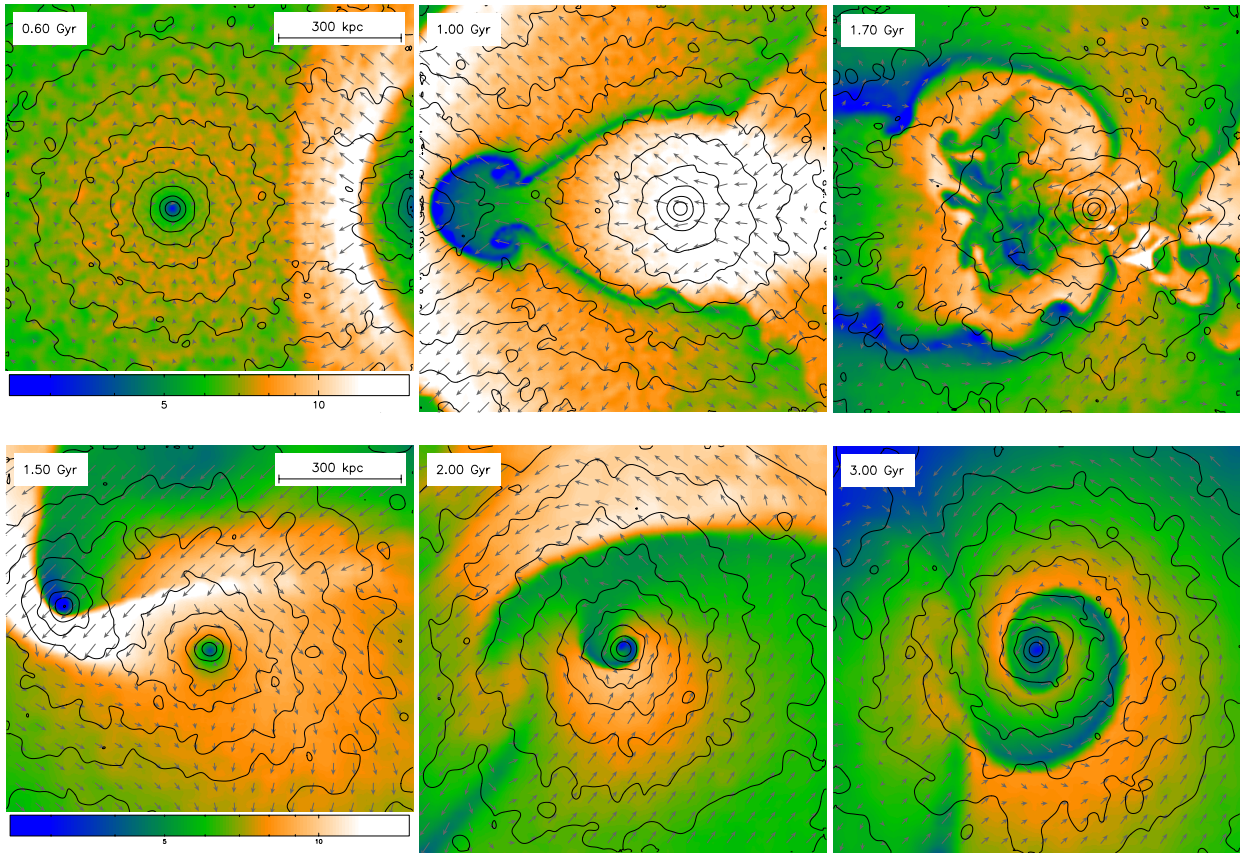


FIG. 15.— Collisions with different initial impact parameters, for  $R = 5$  and DM+gas subcluster run. Head-on collision (top) and encounter with  $b = 1$  Mpc (bottom). The top run has  $N = 10^7$  gas particles, the bottom run has  $N = 10^6$  particles.

low-entropy as near the very center) still forms a flow from the middle of the slingshot front toward the center. The angular momentum of the dense gas behind the slingshot front is now higher (because the angular momentum of the merger is higher), which makes the gas to flow toward the center in a well-pronounced spiral pattern. Close examination shows that this spiral flow is a limiting, very lopsided case of the staggered mushroom-like structures that we saw in Figs. 7 and 9 (see §3.3).

Between the time when the slingshot cold front moves beyond  $r = 500$  kpc and the return of the subcluster, there is a 1–1.5 Gyr period when the cluster looks relaxed on a 1 Mpc scale, except for the central spiral cold front (e.g., the 3.0 Gyr panel in Fig. 15). Around  $t = 4.0$  Gyr, the subcluster makes a second passage with a smaller angular momentum, hits close to the center and its gas core disturbs the cold fronts. A few gigayears later, we have a relatively relaxed cluster with a sloshing core similar to the one in our  $b = 500$  kpc run (the 4.8 Gyr panel in Fig. 9), except its central gas is now a mixture of gases from both subunits.

To summarize, minor mergers ( $R \gtrsim 5$ ) with relatively large initial impact parameters ( $b \gtrsim 500$  kpc, corresponding to pericentric distances of a few hundred kpc) can easily cause sloshing of the innermost cool, dense gas of the main cluster around the minimum of the gravitational potential, giving rise to “sloshing” cold fronts. For mergers with a DM+gas subcluster, there are periods (albeit relatively short) when the system appears relaxed on large scales and the most visible features are these cold fronts. In general, the bigger the mass ratio and the bigger the impact parameter, the less violent is the large-scale disturbance and the more regular the central cold front

structure (with the caveat that eventual infall of the cool gas stripped from the subcluster disturbs it faster if the subcluster is less massive). For DM-only subclusters, a merger with any reasonable mass ratio and impact parameter would look relaxed.

## 6. NUMERICAL EFFECTS

### 6.1. Resolution

Before proceeding to discussing the above results, we need to address several numerical issues. First, we would like to check whether the sharp edges that we see in the temperature distribution are indeed discontinuities (at least at our resolution) or just steep gradients. This can be done by comparing the width of these features with the code resolution. We selected an interesting moment in our default DM+gas subcluster run ( $t = 1.7$  Gyr, see the 1.67 Gyr panel shown in Fig. 9) with two cold fronts developed in regions of different gas densities, and reran the whole simulation with a lower number of gas particles,  $10^6$  and  $10^5$  (compared to the default  $10^7$ ). Initial conditions were identical.

Figure 16 shows the temperature profile along a line passing approximately perpendicularly through both cold fronts. Typically, SPH simulations can resolve structures larger than twice the smoothing scale  $h$ , which in our experiments roughly corresponds to the distance to the 64-th neighbor. As can be seen in Fig. 16, the width of our temperature gradients is indeed close to (or even smaller than)  $2h$  at the locations of the cold fronts, shown by the horizontal bars. As the resolution improves, both features become correspondingly narrower. Although this does not guarantee that increasing the number of particles still further will not eventually resolve



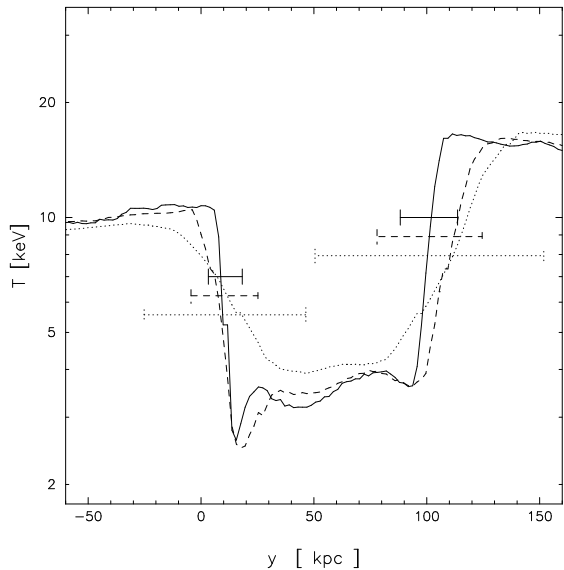


FIG. 16.— Temperature across the cold fronts at  $t = 1.7$  Gyr in the encounter with a DM+gas satellite described in §4. Dotted, dashed and solid correspond to the same simulation, run with  $N = 10^5$ ,  $10^6$  and  $10^7$  gas particles. Horizontal lines indicate the resolution of each experiment, computed as twice the SPH smoothing length at  $y = 7$  and 100 kpc. The widths of both fronts are equal to the resolution in all cases.

them, it strongly suggests that they are genuine discontinuities and not finite gradients.

In any case, it is encouraging that both cold fronts are present in the same places at the same time at all 3 resolutions. Furthermore, the  $N = 10^6$  profile is very similar to that from our default  $N = 10^7$  experiment, except for the gradient widths. This suggests that we have achieved numerical convergence. It is also clear that  $N = 10^5$  gas particles is not enough to model the central cold fronts.

It is interesting to compare our linear resolution with the electron mean free path due to Coulomb collisions,

$$\lambda_e \approx 23 \text{ kpc} \left( \frac{T}{10^8 \text{ K}} \right)^2 \left( \frac{n_e}{10^{-3} \text{ cm}^{-3}} \right)^{-1}, \quad (10)$$

where  $n_e$  is the electron number density (e.g., Sarazin 1988). In the absence of magnetic fields, this is the minimum scale at which the hydrodynamic approximation is applicable. In reality, the ICM is magnetized and collisionless, so the true mean free path is significantly smaller (which was shown observationally for the cold front in A3667, Vikhlinin et al. 2001). Figure 17 shows  $\lambda_e$  from eq. (10) for our fiducial main cluster, along with the numeric resolution for our  $10^7$  particle runs. Throughout the interesting radial range, our numeric resolution element is bigger, so we do not yet have to worry about what happens in the intracluster plasma on a microscopic level. Future increases in numeric resolution (e.g., dotted line in Fig. 17 for  $10^9$  particles) might pose such questions.

On the other hand, Figure 17 also shows that we may be underestimating the amount of small-scale instabilities and turbulence, because our numeric resolution essentially imposes an artificial damping scale for them. This may be important for the survival of cold fronts, because as we saw in §4, they are disrupted by turbulence (at least on those scales at which turbulence does occur in our simulations). It is instructive to evaluate the characteristic Reynolds numbers in our simulations. For an ideal gas, it is  $\text{Re} \sim Md/l$ , where  $M$  is the Mach number of the flow,  $d$  is the characteristic linear scale and  $l$

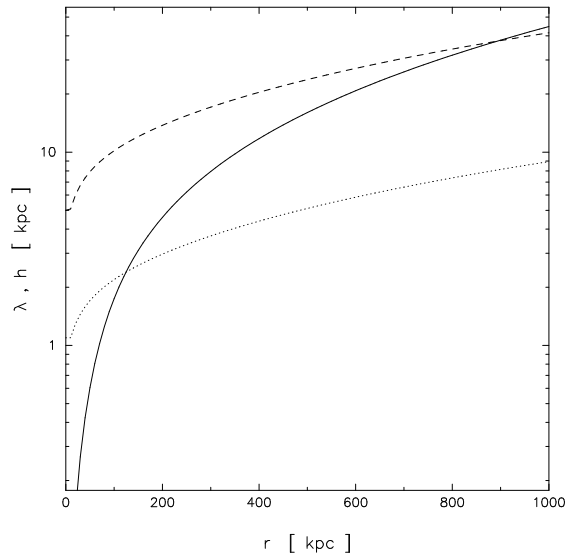


FIG. 17.— Mean free path of the electrons (solid lines) for our  $1.4 \times 10^{15} M_\odot$  cluster with a Hernquist dark matter halo and a cool core, compared to the resolution of our simulations with  $N = 10^7$  SPH particles (dashed line) and a hypothetical experiment with  $N = 10^9$  (dotted lines).

is the mean free path of the gas particles. Turbulence can develop when  $\text{Re} \gtrsim 10$ . At the crudest approximation, we may substitute our linear resolution (Fig. 17) for  $l$ . Then looking at the later panels in Fig. 7 (the DM infall case), Reynolds numbers for the flow around the cool edge features are in the range 3–6, taking the scale of those features as  $d$ . So at our resolution, turbulence cannot develop there. In the gas subcluster run,  $\text{Re} \sim 30$  on a 0.5 Mpc scale, and the destructive effects of turbulence on the cold fronts can indeed be seen in Fig. 9.

## 6.2. Artificial viscosity

Apart from the resolution, there is a more insidious numerical effect, recently pointed out by Dolag et al. (2005), that might affect our results. The SPH formalism resorts to artificial viscosity in order to properly model shock waves. Artificial viscosity tends to erase structures in the velocity field and suppress turbulence. A comparison between the artificial viscosity implemented in GADGET with the new scheme proposed by Dolag et al. (2005, see their Fig. 9) shows that turbulence increases in the latter and tends to break up the fluid interfaces corresponding to our stripping-induced cold fronts. Judging from the apparent magnitude of the effect in Dolag et al. (2005), sloshing-induced cold fronts should still form in the cores if one uses the improved scheme, but their structure may be more irregular and the survival time shorter than suggested by our results. On the other hand, our cold fronts, both sloshing and subcluster-stripping types, have regular shapes very similar to those observed in real clusters (§7.1 below), suggesting that physical viscosity in real systems may not be negligible. This merits a detailed investigation in future works (and may even help to measure the viscosity in the ICM).

The artificial viscosity also increases the entropy of the gas in locations of a steep velocity gradient. To quantify this effect in our simulations, in Fig. 18 we plot the relative entropy increase of SPH particles,  $S(t)/S(0)$ , for the encounter with the pure DM satellite (§3). In this run, the subcluster wake becomes a weak shock only after pericentric passage, so the entropy in the central region should stay constant through-

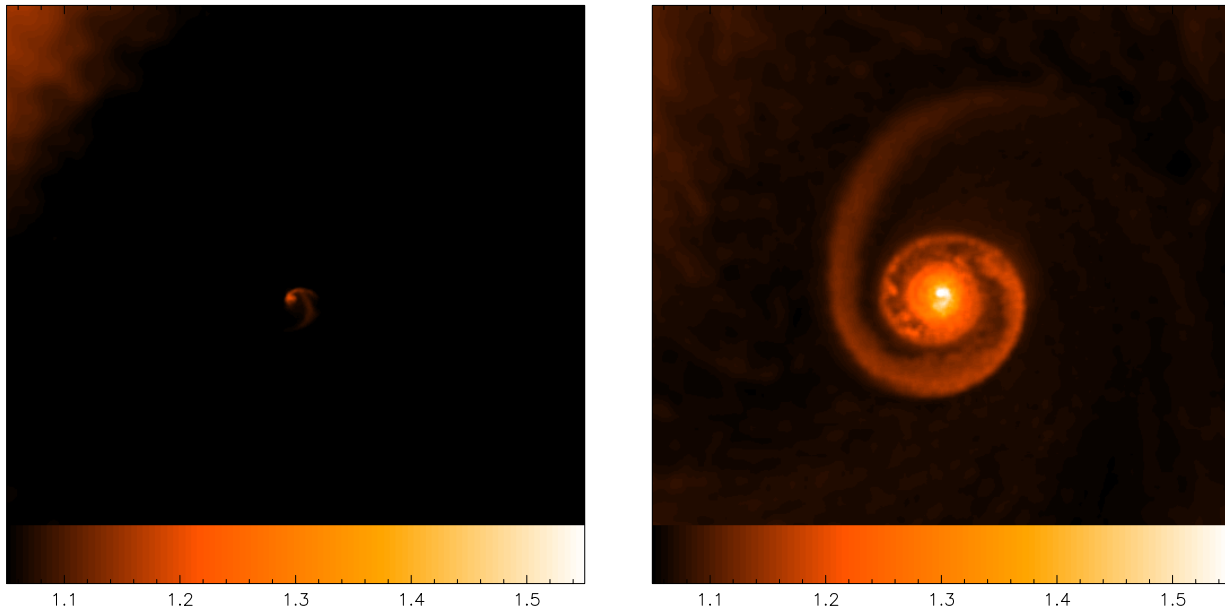


FIG. 18.— The ratio of the gas entropy increase relative to the initial entropy (a numeric artifact), for DM-only run, at  $t = 2.0$  and  $6.0$  Gyr.

out the whole simulation. We can see, however, that artificial viscosity injects a small amount of “numerical entropy” into the ICM at the locations of the cold fronts, which often exhibit velocity shear. At  $t = 2$  Gyr, this results in a  $\sim 20\%$  increase in the entropy of some particles. The effect becomes stronger as the large spiral structure develops. By 6 Gyr, for some particles the specific entropy has increased by 50% from its original value. At constant pressure (imposed by hydrostatic equilibrium), that translates into temperatures higher, and densities lower, by 12% and 28% with respect to their true values. As we mentioned in §3.3, this may inhibit sinking of the dense gas from the cold fronts back toward the center, and therefore make the outer parts of the cool spiral structure more prominent. However, compared to the steep overall gas density gradient in the cluster, this artificial density change is small and should not affect the picture qualitatively.

Finally, in the first panel of Fig. 9, one may notice a narrow hot strip along the lower boundary of the gas stripped from the subcluster. It is seen more prominently in the corresponding X-ray image (the first panel in Fig. 22, slightly shifted in time) as a narrow low-brightness strip separating the two subclusters. Its width is a couple of resolution elements. This strip contains high-entropy gas from the outskirts of the main cluster that the subcluster has dragged inside, due to the fact that the gas cannot flow freely along the interface. This “viscosity” appears to be a resolution effect. It may or may not reflect what happens in real clusters, but it should not affect our present results in any qualitative way.

## 7. DISCUSSION

### 7.1. Comparison with observations

Our simulations have shown that mergers with a wide range of parameters, even with the subcluster lacking any gas at all, easily set off sloshing in the cool central gas and generate cold fronts with density and temperature jumps of a factor of 2 and more, the amplitudes observed in real clusters. However, observers deal with projected X-ray brightness and temperatures, so it is interesting to see if our simulated clusters would look similar in projection.

To match *Chandra* images and spectra, we have constructed

X-ray surface brightness and temperature maps according to the spectral weighting scheme described in Vikhlinin (2005). The X-ray emission of each particle is computed as

$$L_i = m_i \rho_i c(T_i), \quad (11)$$

where  $m_i$ ,  $\rho_i$  and  $T_i$  are the mass, density and temperature of the SPH particle and  $c(T)$  is a function containing the *Chandra* sensitivity to thermal plasma spectra (Vikhlinin 2005). To obtain the temperature that an observer fitting a spectrum from a certain cluster region with a single-temperature model would derive, the gas temperatures along the line of sight are weighted proportional to

$$w_i = L_i T_i^{-0.875}. \quad (12)$$

X-ray luminosities and temperatures have been projected along each of the three main axes of the simulation box and then smoothed with the two-dimensional kernel

$$W(u, v) = \left(\frac{1}{2} - \frac{u-u_i}{h_i}\right) \left(\frac{1}{2} + \frac{u-u_i}{h_i}\right) \left(\frac{1}{2} - \frac{v-v_i}{h_i}\right) \left(\frac{1}{2} + \frac{v-v_i}{h_i}\right) \quad (13)$$

where  $u$  and  $v$  are projected coordinates and the smoothing length  $h_i$  is inversely proportional to the cubic root of the density of each particle, computed by the FIESTAS algorithm (Ascasibar & Binney 2005).

#### 7.1.1. Small-scale X-ray and temperature images

Figure 19 shows X-ray brightness and temperature for three projections of the central 250 kpc region of the cluster from our pure-DM subcluster run (§3) at  $t = 2.1$  Gyr, a moment when the spiral structure is prominent. All three edges seen in the corresponding temperature slice (Fig. 7) exhibit density and temperature jumps by a factor of 2. In projection, a spherical discontinuity becomes a discontinuity in the gradient of the respective quantity. So as expected, the features are less prominent in projection, but still clearly seen (with the help of the quadratic dependence of the X-ray brightness on gas density). The spiral edge pattern projected along the  $x$  axis looks like several concentric arcs, while the  $y$  projection is less favorable and barely reveals only the two central discontinuities.

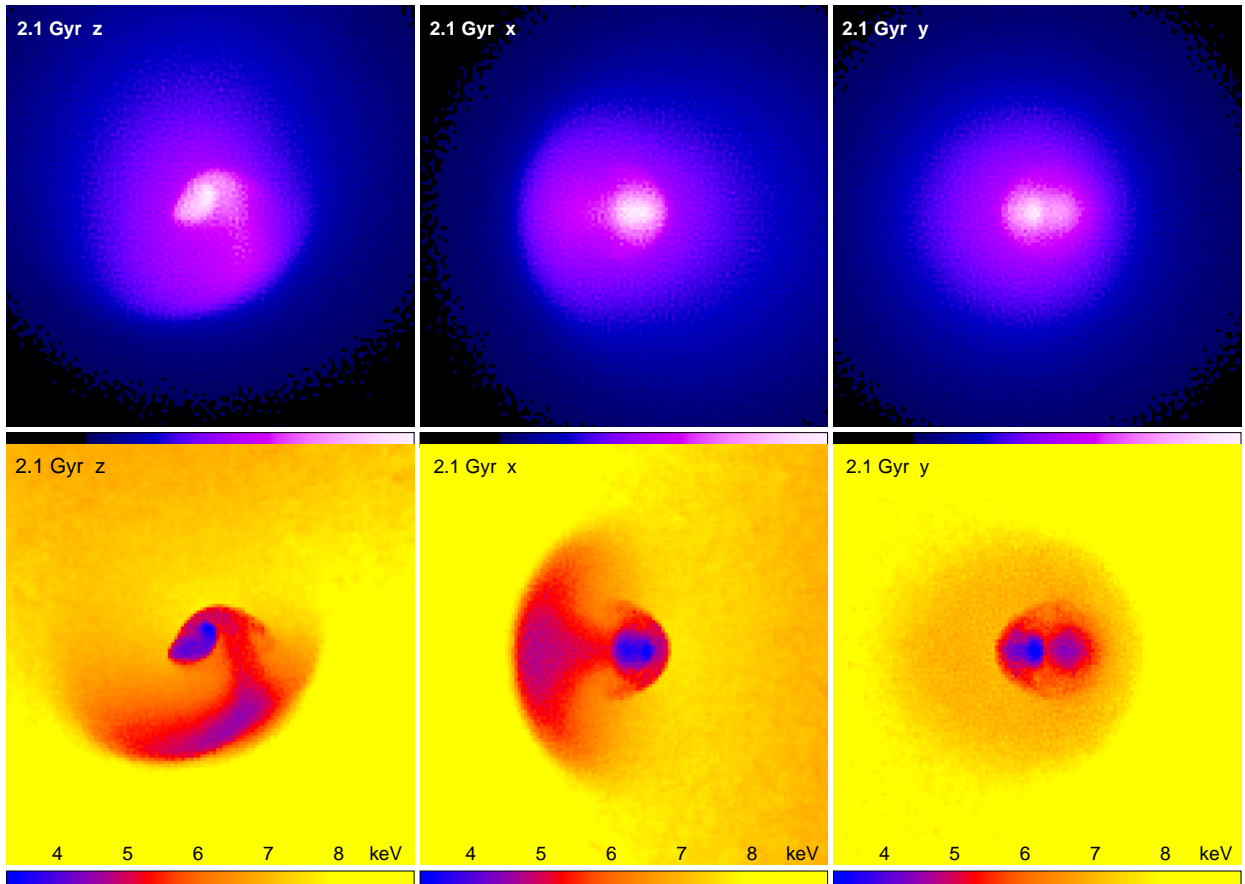


FIG. 19.— X-ray images (top) and projected temperature maps (bottom) of the central region (0.25 Mpc panel size) for the run shown in Fig. 3 ( $R = 5$ , pure DM subcluster), as seen from three different directions. The  $z$  projection is the merger plane projection shown in Fig. 3. In  $x$  projection, the spiral structure looks like the often-observed concentric arcs.

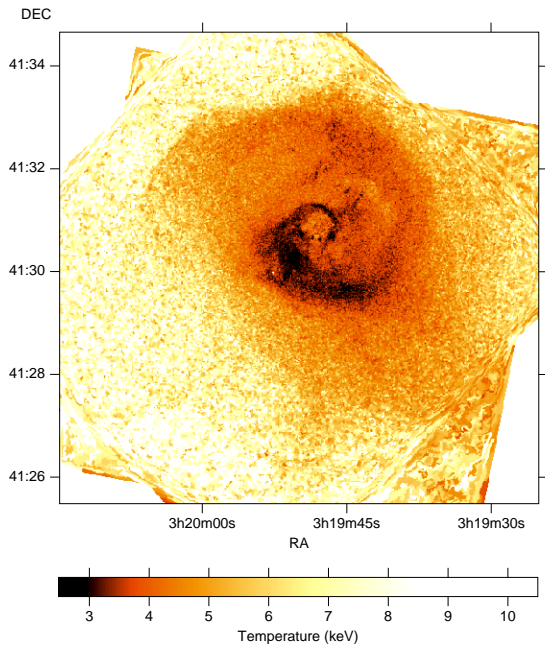


FIG. 20.— *Chandra* projected gas temperature map of the central region of the Perseus cluster, the most detailed map of any cluster obtained to date (reproduced from Fabian et al. 2005b). A large-scale spiral structure such as those in our simulations can be clearly seen. (A  $\sim 1'$  diameter cool ring at the innermost end of the spiral is a boundary of an AGN bubble, unrelated to sloshing.) The linear size of the map is 200 kpc.

The spiral-like structures such as that in the  $z$  projection in Fig. 19 look very similar to those observed in X-ray images of real clusters, such as A2029 and especially Ophiuchus (Fig. 1). The 2.1 Gyr panel of Fig. 7 is probably the best illustration of the gas flows inside the Ophiuchus core. Sufficiently detailed temperature maps for real clusters are much harder to come by, but a 1 Ms *Chandra* observation of Perseus, the best-exposed cooling flow cluster to date, reveals just such a spiral temperature structure, with several edges at different scales (Fig. 20, reproduced from Fabian et al. 2005b; a larger-scale map from *XMM* can be found in Churazov et al. 2003). The  $\sim 1'$  diameter black ring in the very center is a cool boundary of the AGN bubble unrelated to our subject, but the structure on larger scales bears a remarkable resemblance to that in Fig. 19. A temperature map for the core of another cooling flow cluster, Centaurus (Fabian et al. 2005a), looks like the  $x$  projection in Fig. 19.

### 7.1.2. Large-scale X-ray images

Since the primary motivation for this study is to explain cold fronts in relaxed clusters, now we will check how relaxed our simulated clusters look on larger scales. Figure 21 shows 1 Mpc X-ray images for several interesting moments of our merger with a DM-only subcluster (§3 and Fig. 3). Most of the time, the only disturbances seen in the images are the central cold fronts. For several brief periods, when the DM satellite crosses the cluster, it generates a subtle conical wake (first and last panels), but the subcluster spends most of the time in the outskirts. This simulation looks very much like

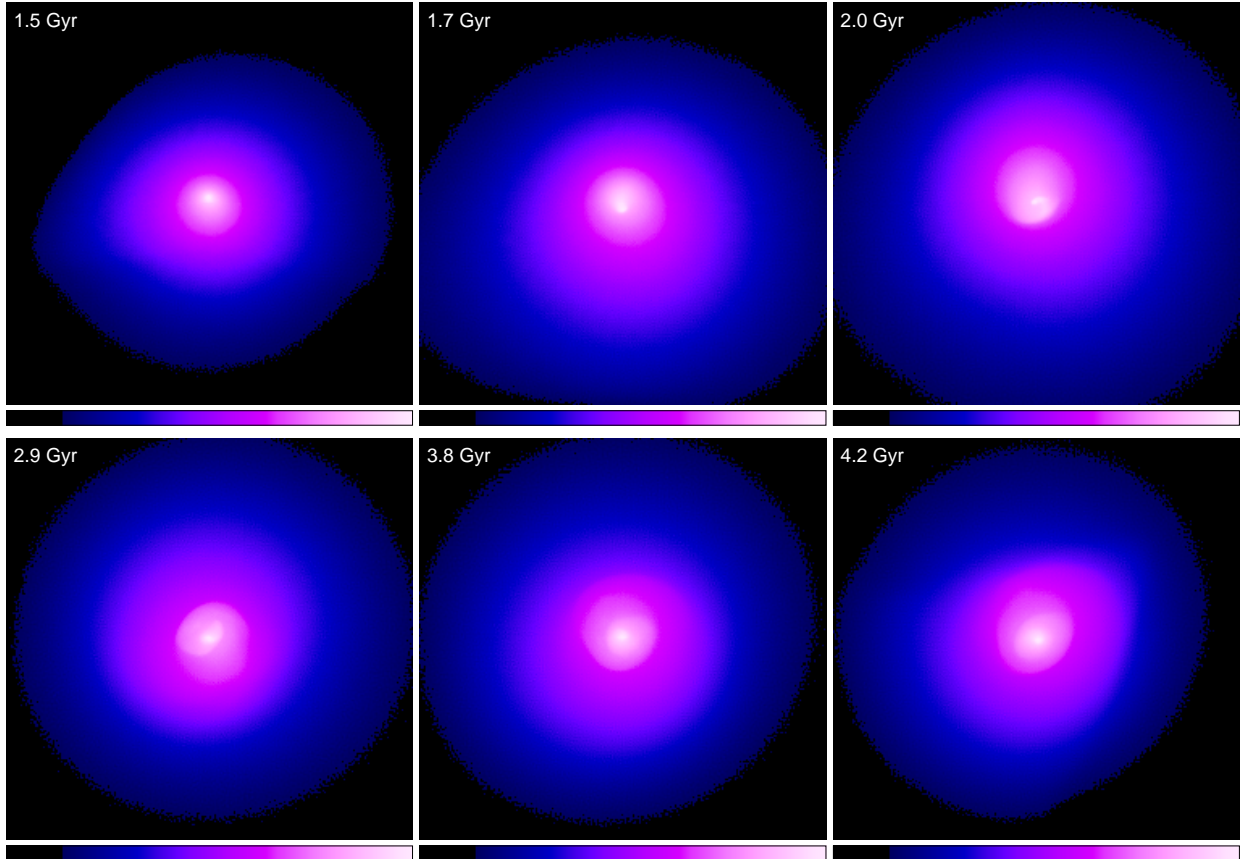


FIG. 21.— Projected X-ray brightness for the merger shown in Fig. 3 ( $R=5$ , pure DM subcluster). The panel size is 1 Mpc. Brightness scale is logarithmic and the same in all panels. With the possible exception of short moments of the subcluster flyby generating a conical wake (1.5 Gyr and 4.2 Gyr), the cluster stays very symmetric on large scales; the only structure is edges in the center.

the most relaxed cooling-flow clusters in the real world, such as A2029 (compare its image in Fig. 1 and the 2.0 Gyr panel in Fig. 21) and A1795.

Figure 22 shows a merger with the DM+gas subcluster (§4, Fig. 9). At early stages, it generates a wealth of prominent cold fronts, including a ram pressure stripping front in the subcluster, a large “slingshot” front 0.3–0.6 Gyr after the core passage, and sloshing fronts in the center around the same and later time. However, it also generates a strong general disturbance and asymmetry. At all stages, except long after the merger (the last panel), such disturbance will be obvious in any well-exposed X-ray observation. As discussed in §5.4, if the satellite is less massive and/or has a greater impact parameter, there may be relatively short periods (of the order of 1 Gyr) when disturbances in the  $r < 500$  kpc region (other than the central cold fronts) are weak and the cluster may pass as “relaxed”. However, we conclude that sloshing in the cores of the relaxed clusters is most probably caused by near-center passages of pure-DM subhalos preserved within the cluster.

## 7.2. Other observable effects

### 7.2.1. Abundance discontinuities

The mergers and processes modeled here to explain the central cold fronts have other observable effects. We expect discontinuities in the metal abundance to accompany the temperature discontinuities, even if the satellite did not contribute gas with a different abundance, or any gas at all. They would result from the centrally peaked initial abundance profiles, observed in most, if not all, cooling-flow clusters (e.g., Vikhlinin et al. 2005). Sloshing brings into contact the gases from dif-

ferent initial radii and should create abundance jumps just as it creates the temperature jumps (§7.4 and Fig. 23). Such abundance jumps at the cold fronts are indeed seen in Centaurus (Fabian et al. 2005a) and Perseus (Sanders et al. 2004), although Dupke & White (2003) reported no significant abundance discontinuity in A496 from a less statistically accurate measurement.

### 7.2.2. cD oscillations

The centers of all cooling flow clusters contain giant cD galaxies, which often exhibit peculiar line-of-sight velocities up to a few hundred  $\text{km s}^{-1}$  relative to the average velocity of other cluster galaxies (e.g., Oegerle & Hill 2001). If the cD galaxy sits exactly at the cusp of the DM distribution (as is most likely), we expect it to start oscillating along with the DM peak after each subcluster flyby, as shown in Fig. 4. Gas sloshing and cD peculiar velocities can thus be caused by the same minor mergers. Indeed, the observed cD peculiar velocities are of the order of what we see in our simulations (e.g., the velocity of the DM peak during the subcluster flyby in Fig. 4 is around  $200 \text{ km s}^{-1}$ ).

A peculiar velocity of the cD galaxy, and perhaps a disturbed shape of its extended stellar envelope, could be tell-tale signs of a close encounter with a massive subcluster. Such signatures may be expected in cold fronts caused by gasless satellites. At the same time, as we have seen above, cold fronts with similar amplitudes may also be caused by hydrodynamical disturbances (i.e. a shock wave) from a gas subcluster orbiting farther away from the center, which may leave the cD galaxy undisturbed. In principle, this difference may

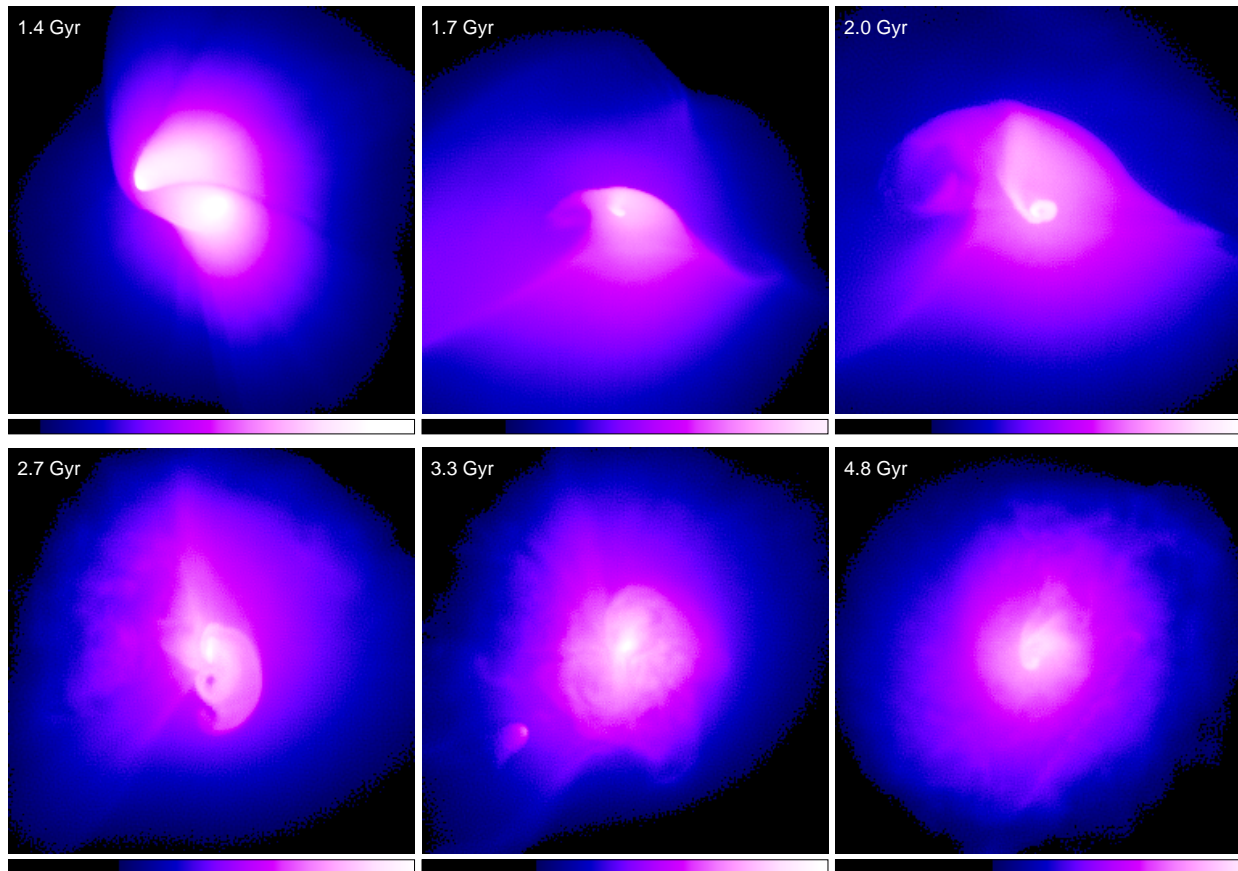


FIG. 22.— Projected X-ray brightness for the merger shown in Fig. 9 ( $R = 5$ ,  $b = 500$  kpc, DM+gas subcluster). The panel size is 1 Mpc. Brightness scale is logarithmic; color scale is adjusted in each plot to emphasize interesting features. The cluster is very disturbed on all scales; it needs 3–4 Gyr after the first core passage to start looking relaxed on large scales (last panel).

be used to determine the cause of the central disturbance in a particular cluster. A quantitative analysis is beyond the scope of the present paper.

### 7.3. Minor mergers or AGN explosions?

Our simulations have shown that it is very easy to set off sloshing of the cool gas in the cluster center. In principle, it could be caused by any disturbance other than a minor merger. For example, an AGN blowing a bubble in the dense gas, such as those seen in many cooling flow clusters (e.g., McNamara et al. 2000) may set off gas sloshing, provided the explosion was offset from the density peak, as seen in simulations by Quilis et al. (2001). It would be interesting to model this process in more detail. However, we can put forward two arguments against AGN explosions being a prevalent mechanism for the central cold fronts. First, it is not clear how an AGN could provide angular momentum to the gas, which is necessary to produce the often-observed spiral fronts. Second, the ubiquitous cD peculiar velocities mentioned above indicate that minor mergers such as those simulated here occur often, and should generate long-lived sloshing via the mechanism presented here, regardless of whether there are other mechanisms at work.

Note that in some clusters showing X-ray edges near the center, those edges may be an altogether different phenomenon. In the Hydra-A cluster, the edge appears to be a weak shock propagating in front of a large AGN-blown bubble (Nulsen et al. 2005). Such edges look somewhat differently from the “sloshing” edges considered here, spanning a larger sector (in Hydra-A, it can be traced almost all the way

around the cluster core). In addition, very subtle brightness edges or “ripples” observed in the core of the Perseus cluster have been attributed to sound waves from the central AGN explosions (Fabian et al. 2005).

### 7.4. Physical origin of contact discontinuities

Our simulations showed that gas sloshing in the cluster center generates sharp contact discontinuities in the gas. We also saw, along with authors of many earlier simulation works, that motion of a gas subcluster creates a discontinuity at its front. Here we would like to address a question which was not clearly explained in the literature — how exactly an initially continuous gas distribution becomes a sharp contact discontinuity. Ram pressure stripping is usually quoted as the agent (e.g., Markevitch et al. 2000; Vikhlinin et al. 2001). It was shown that inside a cold front in A3667, the azimuthal distribution of the gas pressure closely follows the pressure of the hotter gas flowing around the front, if one models the velocity field around the spherical front and uses the Bernoulli equation (Vikhlinin & Markevitch 2002). This indicates that there is pressure equilibrium across the front and therefore its shape is stationary or at least evolves slowly (as opposed, for example, to an expanding bubble). It is easy to understand how stripping by such a tangential gas flow around an infalling dense gas subcluster may remove the outer layers of the subcluster’s gas until it reaches the radius where the pressure in the cold gas equals the pressure outside. However, at the forward tip of the front (the stagnation point), there is no tangential gas flow and no such stripping, yet the fronts are just as sharp there.

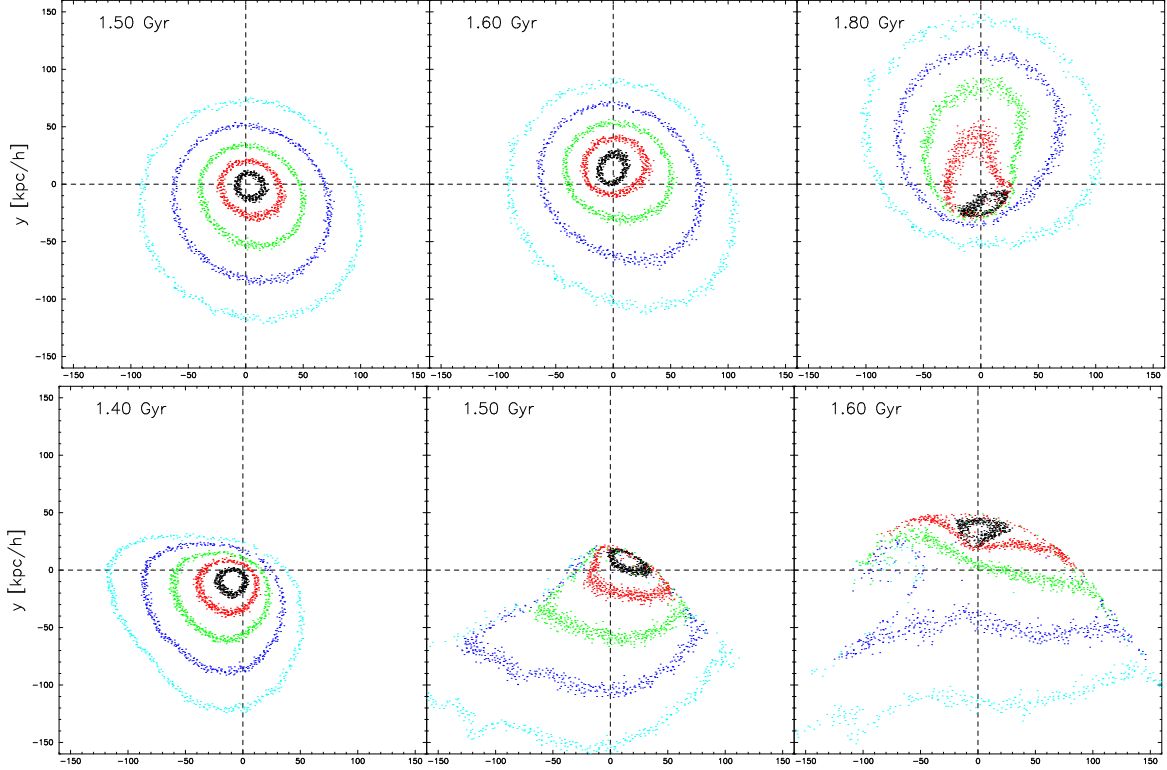


FIG. 23.— Evolution of initially concentric SPH particles during the encounter with a DM-only satellite as in Fig. 3 (top) and with gaseous satellite as in Fig. 9 (bottom), showing the emergence of a sharp density discontinuity. The cross shows the DM peak.

When the subcluster has a gaseous component, ram pressure is exerted by the shocked ICM gas and then by the gas stripped from the subcluster, so one could argue that there are discontinuities in the ICM to begin with. However, in our DM-only subcluster run, there is no shock and no other gas, the gas density and velocity distributions are perfectly continuous until the sloshing starts.

The moment when the first contact discontinuities emerge in the main cluster core is shown in Fig. 23, where top panels show our simulations with the DM-only subcluster and bottom panels show the one with the gas subcluster. The figures show the positions of individual SPH gas particles extracted from initially concentric annuli around the main cluster center, in a slice along the merger plane. It is instructive to compare this plot with the figures showing the velocity field, Figs. 5 and 7 for the DM-only subcluster and Fig. 9 for the gas subcluster. For the DM-only run, 1.55 Gyr is the approximate moment when the main core reverses the direction of motion w.r.t. the surrounding gas and starts experiencing ram pressure at its downward side. The net force from the ram pressure is the same for each cubic centimeter of the gas in the core (near the symmetry axis and assuming subsonic motions). Therefore, denser gas experiences a smaller resulting acceleration. This quickly produces a velocity gradient inside the core along the direction of the force. The lower-density, outer layer of the core gas (red and green dots) is then squeezed to the sides from the region where the ambient flow eventually meets the dense gas for which the density-proportional gravity or inertial force prevails over the area-proportional ram pressure force (black dots; 1.80 Gyr panel).

The same process occurs in the run shown in lower panels of Fig. 23. At 1.4 Gyr, the core starts experiencing ram pressure (much stronger than in the case above), and by the next snapshot the velocity gradient along the ram pressure force

has brought the dense gas in contact with the outer gas. By the next snapshot, the process is repeated on a smaller scale, when the densest gas turns around and again starts moving toward the center against an ambient flow.

One may note that in both cases, the first discontinuity arises right after the dense gas overshoots the DM peak. Although this increases the temperature contrast due to adiabatic expansion of the dense gas as it moves to a lower-pressure environment, it is not a necessary condition and is largely a coincidence. Indeed, sharp contact discontinuities form in the infalling subcluster (e.g., the 1.39 Gyr panel in Fig. 9) and in our sloshing core (e.g., the 1.67 Gyr panel) without overshooting the DM core. We conclude that whenever a smooth gas density peak encounters a flow of ambient gas (caused by subcluster infall, shock passage, sloshing, etc.), a contact discontinuity quickly forms by “squeezing out” the gas layers near the future stagnation point that are not in pressure equilibrium with the flow. Away from the axis of symmetry of the cold front, such gas is stripped by the shear flow.

### 7.5. Comparison with previous works

A number of earlier hydrodynamic simulations have been devoted to the origin of cold fronts in clusters since their discovery in real systems. Cold fronts have been seen in several cosmological experiments, always as a consequence of merging activity (e.g. Bialek et al. 2002; Nagai & Kravtsov 2003; Mathis et al. 2005). The fronts seen in those simulations are analogous to our large-scale discontinuities separating the ICM of the two merging clusters — the ram pressure stripping front in the infalling subcluster, and the “slingshot” front in the main cluster after the first core passage (Fig. 9). The small-scale sloshing-induced cold fronts described in this work have never been reported in a cosmological setting. This is not surprising given that, on one hand, the resolution of

these works is substantially lower than the experiments presented here. On the other hand, in realistic cosmological simulations, it is often difficult to disentangle the effects of concurrent physical processes. For this reason, idealized simulations with controlled initial conditions are very helpful in deriving a physical interpretation of the observed phenomenology.

Several earlier idealized simulations obtained results relevant for the phenomenon considered here. Heinz et al. (2003) used 2D simulations to model a passage of a shock wave through an isothermal  $\beta$ -model gas core in a stationary gravitational potential. Their core developed a cold front and a circulation pattern where the lower-entropy gas was flowing from the center toward the front and was then redirected to the sides along the front surface. We do see a similar circulation pattern forming in our simulations whenever the cluster core is subjected to an ambient flow (e.g., Fig. 7). In our case, however, the initial gas core is not flat but resembles a cooling flow with a steep entropy decline toward the center, and the gas is supported by a cuspy DM profile. This produces additional reverse flows of the lowest-entropy gas from the front toward the center along the filaments forming via RT instability. This was absent in the Heinz et al. (2003) setup.

Churazov et al. (2003) and Fujita et al. (2004) used 2D simulations to show that a weak shock or acoustic wave propagating toward a cooling flow can displace the cool gas from its equilibrium in the gravitational potential well. According to Churazov et al., the cool gas then starts oscillating in the potential well with different periods for the gas at different radii, which produces a series of cold fronts at different radii at the opposite sides of the core. The cold fronts are locations of the apocenters of oscillations where the gas spends most of the time. This is approximately what we see, except that the disturbance in our setup is created by a subcluster flyby. We also find that cold fronts are not the end points of the gas oscillations (which was also proposed in the original paper by Markevitch et al. 2001), but rather structures continuously moving outward through a combination of gas sloshing and circulation inside the front (Figs. 7 and 14 and §3.3).

Finally, the work that used the setup closest to ours is Tittley & Henriksen (2005), who carried out three-dimensional numerical simulations of off-center mergers with mass ratios 10 and 30. The mergers were selected from a cosmological run. They propose that the central cold fronts arise as a result of oscillations of the main cluster’s DM peak initiated by the passage of the substructure. In their scenario, the central gas is dragged along by the DM peak and cold fronts form due to compression of the gas on the forward side. They did not actually see the cold fronts because of insufficient resolution ( $N \sim 10^4 - 10^5$  particles, compared to our  $10^7$ ). In our DM-only subcluster run, the initial decoupling of the cool gas from the DM peak is indeed caused by a swing of that peak during the subcluster flyby (§3.1). However, the subsequent gas sloshing, which generates cold fronts, proceeds with a period much shorter than oscillations of the DM core (§3.2). When the infalling subcluster has gas, we find that the initial gas-DM displacement is also mostly a hydrodynamic effect (§4).

## 8. SUMMARY

We used high-resolution hydrodynamic simulations of idealized cluster mergers in order to determine if and how they can cause the ubiquitous cold fronts observed by *Chandra* in the centers of many “relaxed” clusters with cooling flows.

Several numerical experiments have been carried out, varying the mass ratio of the merger, the initial impact parameter, and the shape of the central gravitational potential. We also tried a merger with a dark matter subcluster devoid of any gas. Our initial gas density and temperature profiles match closely those observed in real cooling-flow clusters, such as A2029. As a test, we also tried a cluster with an isothermal gas core.

Our results show that mergers with small subclusters easily set off sloshing of the cool gas in the main cluster central potential minimum, which gives rise to cold fronts very similar to those observed in real clusters. The necessary conditions for such sloshing are the presence of an initial steep entropy drop in the center (such as that in cooling flows) and that the merger does not completely destroy the cool core in a head-on impact. The presence of a central DM cusp is not necessary, although it does make the cold front structure look more realistic.

It is difficult to set off central gas sloshing without causing an obvious global disturbance in the cluster. When the infalling subcluster has gas, we observe shocks, a cold front in the subcluster, gas stripped from the subcluster, and a large-scale “slingshot” cold front propagating from the center of the main cluster and separating the ICM of the two halos. If the main cluster had a cooling flow, we additionally see sloshing in the center. The cool gas stripped from the subcluster eventually falls into the center of the main cluster and disturbs any coherent motions there. We find that minor mergers with mass ratios  $R \gtrsim 5$  and large impact parameters ( $b = 0.5 - 1$  Mpc, corresponding to distance during core passage of 100–400 kpc) may produce relaxed-looking clusters with the visible disturbance limited to the central sloshing, but only for brief ( $\sim 1$  Gyr) periods or very late in the merger.

However, if the infalling subcluster did not have any gas during core passage (e.g., it was completely stripped at an early stage), the only noticeable disturbance during the merger is the central sloshing. The resulting pattern of cold fronts can survive for several gigayears. This type of mergers appears to provide the best fit to the most-relaxed observed clusters with central cold fronts, such as A2029 and A1795.

Gas sloshing is set off when the gas peak is displaced from the DM peak and starts falling back. In the main core, this occurs as a result of a “ram pressure slingshot”, when the core gas is first compressed and displaced by ram pressure, and then it suddenly diminishes. When the infalling subcluster has gas, ram pressure is caused mainly by the passage of the shock. In the DM-only subhalo case, it is caused mostly by the orbital swing of the main DM peak during the subhalo flyby. A gravitational wake created by the DM subcluster in the gas of the main cluster also plays a role in the latter case. In a process similar to Rayleigh-Taylor instability, the densest fraction of the displaced gas quickly turns around and starts falling back toward the potential minimum. It encounters the less-dense gas that is still flowing in the opposite direction, and forms a mushroom-shaped cold front. The mushroom head overshoots the potential minimum, after which the densest gas turns around again and the picture repeats itself at progressively smaller linear scales. This creates the often-observed pattern of near-concentric density edges at different radii on the opposite sides from the center. If the subcluster had a nonzero impact parameter, these edges are not exactly concentric but instead form a spiral pattern, also seen in real clusters. This spiral is just a superposition of the independent edges and does not represent any coherent spiraling motion, at least not initially.

We find that although the lowest-entropy gas indeed sloshes back and forth in the potential minimum, each cold front, once formed, propagates outward from the center and does not “turn around” or “straighten out”. There appears to be a circulation pattern in which the lowest-entropy gas initially forming this cold front, turns around and sinks back towards the center, while being replaced at the front by higher-entropy gas. The caveat here is that details of the long-term evolution of the fronts in our simulations may be affected by a numerical artifact, namely, the spurious generation of entropy by the artificial viscosity inherent to the SPH scheme.

On the other hand, our SPH simulations can trace the origin of gas particles, enabling us to see exactly how the initially continuous gas density and velocity field gives rise to a contact discontinuity. It arises naturally when the gas density peak starts moving and experiencing ram pressure from the ambient ICM gas, which creates an acceleration gradient along the direction of the flow. The highest-density gas, for which the density-proportional gravity or inertial force prevails over the area-proportional ram pressure force, then squeezes the lower-density gas, more easily affected by ram pressure, to the sides and eventually comes into contact with the ambient medium.

We have shown that minor mergers easily create sloshing and cold fronts in the cooling flow clusters. In principle, any gas disturbance may set off sloshing, e.g., AGN explosions, and it would be interesting to model such a process in detail. However, there are arguments against AGN outbursts being a prevalent mechanism. Most notably, the ubiquitous cD peculiar velocities indicate that minor mergers, such as those simulated here, do occur and should generate sloshing via the mechanism presented here.

In a forthcoming paper, we will use these simulations to address the effects of the central gas sloshing on cooling flows and on the total mass estimates derived under the assumption of hydrostatic equilibrium.

We are grateful to L. Hernquist, P. Nulsen, A. Vikhlinin, P. Ortiz, and C. Jones for useful discussions. YA thanks Harvard-Smithsonian Center for Astrophysics for hospitality; all simulations presented in this work have been carried out at the CfA’s Institute for Theory and Computation. The work was supported by NASA grants G02-3164X and G04-5152X and NASA contract NAS8-39073.

## REFERENCES

- Acreman, D. M., Stevens, I. R., Ponman, T. J., & Sakelliou, I. 2003, *MNRAS*, 341, 1333
- Asai, N., Fukuda, N., & Matsumoto, R. 2004, *ApJ*, 606, L105
- Ascasibar, Y. & Binney, J. 2005, *MNRAS*, 356, 872
- Bialek, J. J., Evrard, A. E., & Mohr, J. J. 2002, *ApJ*, 578, L9
- Buote, D.A. and Tsai, J.C., 1996, *ApJ*, 458, 27
- Churazov, E., Forman, W., Jones, C., and Böhringer, H. 2003, *ApJ* 590, 225
- Clarke T. E., Blanton E. L., Sarazin C. L., 2004, *ApJ*, 616, 178
- Dolag, K., Vazza, F., Brunetti, G., & Tormen, G. 2005, (*astro-ph/0507480*)
- Dupke R., White R. E., 2003, *ApJ*, 583, L13
- Fabian A. C., Sanders J. S., Taylor G. B., Allen S. W., 2005, *MNRAS*, 360, L20
- Fabian A. C., Sanders J. S., Taylor G. B., Allen S. W., Crawford C. S., Johnstone R. M., Iwasawa K., 2005, *astro-ph/0510476*
- Fujita Y., Matsumoto T., Wada K., 2004, *ApJ*, 612, L9
- Hallman, E.J. and Markevitch, M. 2004, *ApJ*, 610, L81
- Heinz, S., Churazov, E., Forman, W., Jones, C., & Briel, U. G. 2003, *MNRAS*, 346, 13
- Hernquist, L. 1990, *ApJ*, 356, 359
- Machacek, M., Dosaj, A., Forman, W., Jones, C., Markevitch, M., Vikhlinin, A., Warmflash, A., and Kraft, R., 2005, *ApJ*, 621, 663
- Markevitch M., Gonzalez A. H., David L., Vikhlinin A., Murray S., Forman W., Jones C., Tucker W., 2002, *ApJ*, 567, L27
- Markevitch M., Vikhlinin A., Forman W. R., 2003, in *ASP Conf. Proc.*, Vol. 301, 37 (*astro-ph/0208208*)
- Markevitch M., Vikhlinin A., Mazzotta P., 2001, *ApJ*, 562, L153
- Markevitch et al. 2000, *ApJ*, 541, 542
- Mathis, H., Lavaux, G., Diego, J. M., & Silk, J. 2005, *MNRAS*, 357, 801
- Mazzotta, P., Markevitch, M., Vikhlinin, A., Forman, W. R., David, L. P., & VanSpeybroeck, L. 2001, *ApJ*, 555, 205
- McNamara, B.R., Wise, M., Nulsen, P.E.J., David, L.P., Sarazin, C.L., Bautz, M., Markevitch, M., Vikhlinin, A., Forman, W.R., Jones, C., and Harris, D.E. 2000, *ApJ*, 534, L135
- Nagai, D. & Kravtsov, A. V. 2003, *ApJ*, 587, 514
- Nulsen, P. E. J., McNamara, B. R., Wise, M. W., & David, L. P. 2005, *ApJ*, 628, 629
- Oegerle, W.R. & Hill, J.M. 2001, *AJ*, 122, 2858
- Quilis, V., Bower, R. G., and Balogh, M. L. 2001, *MNRAS*, 328, 1091
- Ricker, P. M. & Sarazin, C. L. 2001, *ApJ*, 561, 621
- Sakelliou, I. 2000, *MNRAS*, 318, 1164
- Sanders J. S., Fabian A. C., Allen S. W., Schmidt R. W., 2004, *MNRAS*, 349, 952
- Sanders J. S., Fabian A. C., Taylor G. B., 2005, *MNRAS*, 356, 1022
- Sarazin, C. L. 1988, *X-Ray Emission in Cluster of Galaxies* (Cambridge: Cambridge Univ. Press)
- Springel, V. 2005, *MNRAS*, 364, 1105
- Takizawa, M. 2005, *ApJ*, 629, 791
- Tittley, E. R. & Henriksen, M. 2005, *ApJ*, 618, 227
- Vikhlinin, A., 2005, *ApJ*, in press (*astro-ph/0504098*)
- Vikhlinin, A. & Markevitch, M. 2002, *Astronomy Letters*, 28, 495
- Vikhlinin, A., Markevitch, M., & Murray, S. S., 2001, *ApJ*, 551, 160
- Vikhlinin, A., Markevitch, M., Murray, S. S., Jones, C., Forman, W., & Van Speybroeck, L. 2005, *ApJ*, 628, 655